Arteriosclerosis, Thrombosis, and Vascular Biology

BASIC SCIENCES

Apolipoprotein A1 Protects Against Necrotic Core Development in Atherosclerotic Plaques: PDZK1-Dependent High-Density Lipoprotein Suppression of Necroptosis in Macrophages

George E.G. Kluck, Alexander S. Qian, Emmanuel H. Sakarya, Henry Quach, Yak D. Deng, Bernardo L. Trigatti

BACKGROUND: Atherosclerosis is a chronic disease affecting artery wall and a major contributor to cardiovascular diseases. Large necrotic cores increase risk of plaque rupture leading to thrombus formation. Necrotic cores are rich in debris from dead macrophages. Programmed necrosis (necroptosis) contributes to necrotic core formation. HDL (high-density lipoprotein) exerts direct atheroprotective effects on different cells within atherosclerotic plaques. Some of these depend on the SR-B1 (scavenger receptor class B type I) and the adapter protein PDZK1 (postsynaptic density protein/Drosophila disc-large protein/Zonula occludens protein containing 1). However, a role for HDL in protecting against necroptosis and necrotic core formation in atherosclerosis is not completely understood.

METHODS: Low-density lipoprotein receptor–deficient mice engineered to express different amounts of ApoA1 (apolipoprotein A1), or to lack PDZK1 were fed a high fat diet for 10 weeks. Atherosclerotic plaque areas, necrotic cores, and key necroptosis mediators, RIPK3 (receptor interacting protein kinase 3), and MLKL (mixed lineage kinase domain-like protein) were characterized. Cultured macrophages were treated with HDL to determine its effects, as well as the roles of SR-B1, PDZK1, and the PI3K (phosphoinositide 3-kinase) signaling pathway on necroptotic cell death.

RESULTS: Genetic overexpression reduced, and ApoA1 knockout increased necrotic core formation and RIPK3 and MLKL within atherosclerotic plaques. Macrophages were protected against necroptosis by HDL and this protection required SR-B1, PDZK1, and PI3K/Akt pathway. PDZK1 knockout increased atherosclerosis in LDLR^{KO} mice, increasing necrotic cores and phospho-MLKL; both of which were reversed by restoring PDZK1 in BM-derived cells.

CONCLUSIONS: Our findings demonstrate that HDL in vitro and ApoA1, in vivo, protect against necroptosis in macrophages and necrotic core formation in atherosclerosis, suggesting a pathway that could be a target for the treatment of atherosclerosis.

GRAPHIC ABSTRACT: A graphic abstract is available for this article.

Key Words: atherosclerosis ■ cardiovascular diseases ■ high-density lipoprotein ■ macrophages ■ necroptosis

Cardiovascular disease is a leading cause of death globally.[1] Atherosclerosis is a chronic inflammatory disease that affects the walls of arteries and represents a major cause of cardiovascular disease.[2] Atherosclerosis is driven by the retention of cholesterol-rich lipoproteins, such as LDL (low-density lipoprotein), in the arterial subendothelial space, followed by their oxidation to form oxidized LDL (oxLDL), and their uptake by phagocytic cells such as macrophages to form lipid engorged foam cells. Advanced

Correspondence to: Bernardo L. Trigatti, Department of Biochemistry and Biomedical Sciences, McMaster University, Thrombosis and Atherosclerosis Research Institute, Hamilton General Hospital Campus, 237 Barton St E, Hamilton, Ontario, L8L 2X2, Canada. Email trigatt@mcmaster.ca
Supplemental Material is available at https://www.ahajournals.org/doi/suppl/10.1161/ATVBAHA.122.318062.
For Sources of Funding and Disclosures, see page 60.

Arterioscler Thromb Vasc Biol is available at www.ahajournals.org/journal/atvb

Nonstandard Abbreviations and Acronyms

ApoA1	apolipoprotein A1
bpV-pic	bisperoxovanadium (PTEN inhibitor)
CETP	cholesteryl ester transfer protein
HDL	high-density lipoprotein
HFD	high-fat diet
h-oxLDL	highly-oxidized low-density lipoprotein
IKKα/β	inhibitor of nuclear factor kappa-β kinase subunit alpha and beta
IPPK	inositol pentakisphosphate 2-kinase
LDL	low-density lipoprotein
LDLR	low-density lipoprotein receptor
MK2	MAPK-activated protein kinase 2
MLKL	mixed lineage kinase domain-like protein
MPM	mouse peritoneal macrophage
PDPK1	phosphoinositide-dependent protein kinase 1
PDZK1	postsynaptic density protein/Drosophila disc-large protein/Zonula occludens protein containing 1
PI3K	phosphoinositide 3-kinase
PTEN	phosphatase and tensin homolog
RIPK3	receptor interacting protein kinase 3
RIPK1	receptor interacting protein kinase 1
SR-B1	scavenger receptor class B type I
TAK1	transforming growth factor beta-activated kinase 1
TBK1	TANK-binding kinase 1
TNFα	tumor necrosis factor alpha
ZVAD	carbobenzoxy-valyl-alanyl-aspartyl-[O-methyl]-fluoromethylketone

Highlights

- Genetic overexpression or knockout of ApoA1 (apolipoprotein A1) has opposite effects on necrotic core development and activation of key necroptotic enzymes within atherosclerotic plaques in mice.
- HDL (high-density lipoprotein) protection against necroptosis requires cell signaling involving the receptor SR-B1 (scavenger receptor class B type 1), the adapter protein PDZK1 (postsynaptic density protein/Drosophila disc-large protein/Zonula occludens protein containing 1), and activation of the PI3K/Akt pathway.
- Restoring PDZK1 in bone marrow–derived cells decreases atherosclerotic plaque and necrotic core sizes, and phosphorylation levels of key enzymes involved in necroptosis.

atherosclerotic plaques are characterized by the presence of large necrotic cores infiltrated by macrophages and surrounded by fibrotic tissue.[3–5] Necrotic cores are composed of cell debris including extracellular lipid and appear to be the result of cell death of macrophages and foam cells.[6] Although atherosclerosis is asymptomatic during its initial stages, advanced atherosclerotic plaques with large necrotic cores are prone to rupture, leading to thrombosis and subsequent myocardial infarction or stroke.[7,8]

The accumulation of excess cholesterol and oxidized lipids as a result of the uptake of oxLDL by macrophages is cytotoxic due to the induction of endoplasmic reticulum and oxidative stress, respectively.[6] These processes are known to lead to apoptosis induction in macrophages, and its contribution to cell death in atherosclerotic plaques has been the subject of intense investigation (reviewed in study by Gonzalez and Trigatti[9]). The significance of macrophage apoptosis on atherosclerotic plaque and necrotic core development may be dependent on the stage of atherosclerosis progress: at early stages, when mechanisms for efferocytosis (the clearance of apoptotic corpses) are intact, macrophage and foam cell apoptosis may play a role in limiting the growth of atherosclerotic plaques; on the other hand, at later stages of plaque evolution, in advanced atherosclerotic plaques, efferocytosis becomes impaired leading to persistence of apoptotic cell corpses and the accumulation of cell debris contributing to the formation of large lesions and necrotic cores.[6,10–12]

An alternative form of programmed cell death, called necroptosis (or programmed necrosis), has also been implicated in necrotic core formation.[13,14] Necroptosis is regulated by RIPK1 (receptor-interacting protein kinase 1) and RIPK3 (receptor-interacting protein kinase 3) and involves the phosphorylation of the MLKL (mixed lineage kinase domain-like) protein. Once phosphorylated, MLKL oligomerizes and forms pores that disrupt the plasma membrane, resulting in necrotic cell death, characterized by cell swelling and rupture and release of cellular proteins that act as danger-associated molecular pattern molecules.[15–19] Several studies show that normal macrophages are susceptible to necroptosis, whereas RIPK3$^{-/-}$ macrophages are protected.[14,20–22] Unlike apoptotic cells, which display "eat me" signals such as phosphatidylserine on their cell surface, promoting their clearance by efferocytes, necroptotic cells either devoid of such signals, or display "don't eat me" signals such as CD47, and are therefore not effectively cleared.[6,23,24] Thus, necroptotic corpses persist, releasing danger-associated molecular patterns and contributing to ongoing inflammation and necrotic core development within

atherosclerotic plaques potentially at all stages of plaque enlargement.[14]

HDLs (high-density lipoproteins) are associated with reduced risk of atherosclerotic cardiovascular disease.[25–34] Mechanistic studies in animal models have demonstrated that increasing HDL concentrations inhibit, while lowering HDL promotes atherosclerosis. For example, overexpression of HDL's main apolipoprotein, apolipoprotein (Apo) A1, as well as intravenous HDL infusions, have both been shown to suppress atherosclerotic development in rodents.[35–42] On the other hand, the targeted inactivation of ApoA1 (apolipoprotein A1), or the overexpression of CETP (cholesteryl ester transfer protein), both of which reduces HDL levels in mice, result in increased atherosclerosis development.[43–46] HDL has long been known to mediate reverse cholesterol transport: that is the transport of excess cholesterol from cells, such as macrophage foam cells in the artery wall, to the liver for biliary excretion or recycling into newly secreted lipoproteins.[47,48] This process is thought to counteract the accumulation of cholesterol in foam cells in the artery wall, protecting against atherosclerosis development. Recent findings have shown that compromising HDL function, such as through modification with reactive aldehydes, can impair some of the atheroprotective functions of HDL in macrophages,[49] as well as impair the cholesterol transport function of HDL via its high-affinity receptor SR-B1 (scavenger receptor class B type I).[50] Interestingly, increasing evidence demonstrates that HDL can activate cell signaling pathways in vascular cells, triggering potentially atheroprotective responses,[51–55] such as protecting macrophages and other cells in culture from apoptosis.[53,56] However, a direct role for HDL in protection against macrophage necroptosis and necrotic core formation has not yet been explored.

We have previously reported that HDL-mediated protection of macrophages against apoptosis induced by a variety of stressors requires PDZK1 (postsynaptic density protein/drosophila disc-large protein/zonula occludens protein containing 1).[56,57] PDZK1 is a cytoplasmic adaptor protein that binds to PDZ-interacting motifs in the cytosolic domains of a variety of cell surface proteins, including the HDL receptor, SR-B1.[58] In hepatocytes, and to some extent in intestinal epithelial cells, the interaction of PDZK1 with SR-B1 stabilizes SR-B1 against degradation.[58–60] In other cell types, such as macrophages and endothelial cells, PDZK1 is not required for stabilization of SR-B1 against degradation, and knockout of PDZK1 does not affect SR-B1 protein levels.[53,59,61,62] In these cell types, knockout of PDZK1 impairs HDL's ability to mediate SR-B1-dependent activation of PI3K (phosphoinositide 3-kinase)/Akt signaling, required to trigger cell migration and protection against apoptosis.[53,56,57,62] However, whether HDL also protects macrophages against necroptosis through a PDZK1-mediated signaling pathway and the consequences of this on necrotic core development in vivo have not been investigated.

In this study, we examined the effects of manipulating HDL levels by either ApoA1 knockout or overexpression of human ApoA1 on high fat diet (HFD)-induced atherosclerosis and necrotic core development in low-density lipoprotein receptor KO mice. In addition, we sought to determine whether HDL protects macrophages against necroptosis and to elucidate the molecular mechanism involved in this process, including the role of PDZK1, in both cultured macrophages and atherogenic mouse models.

MATERIALS AND METHODS

The authors declare that all supporting data are available within the article (and its Supplemental Material).

Mice

All animal procedures were approved by McMaster University's Animal Research Ethics Board in accordance with Canadian Council on Animal Care guidelines. C57BL/6J, 129S1/SvImJ (B6129SF2/J), B6;129S6-Pdzk1tm1Dls/J (PDZK1$^{KO/KO}$), B6.129P2-Apoa1tm1Unc/J (ApoA1$^{KO/KO}$), C57BL/6-Tg (APOA1)1Rub/J (hApoA1TG/TG), B6.129S7-Ldlrtm1Her/J (LDLR$^{KO/KO}$), and B6;129S-Scarb1tm1.1Okoch/J (SR-B1$^{deltaCT/deltaCT}$) were originally purchased from the Jackson Laboratory (Bar Harbor, ME, United States). SR-B1$^{KO/KO}$ mice were originally provided by Monty Krieger (Massachusetts Institute of Technology, Cambridge MA, USA) and were backcrossed >10 generations onto a C57BL/6J background at McMaster University. All mice were maintained as breeding colonies in the David Braley Research Institute Animal Facility at McMaster University. Mice were housed in ventilated cages with automatic watering and had free access to standard laboratory diet (Teklad 18% protein diet, Harlan Laboratories, Mississauga, ON, Canada, CAT#2918-032222M). SR-B1$^{KO/KO}$ mice were maintained by feeding homozygous breeders with a 0.5% probucol in RMH3000 base diet (Purina Lab Diets, distributed by Ren`s Pets, Burlington, ON, Canada, CAT#106258) and weaning the pups onto non-medicated diet. Compound mutant (hApoA1$^{TG/TG}$LDLR$^{KO/KO}$, ApoA1$^{KO/KO}$LDLR$^{KO/KO}$, and PDZK1$^{KO/KO}$LDLR$^{KO/KO}$) lines were generated by crossing the corresponding single KO or TG mice to homozygosity. Genotyping was carried out by PCR of tail biopsy derived DNA (see the Major Resources Table in the Supplemental Material for primer sequences). Mice with malocclusion, hydrocephalus, and/or poor body condition were excluded from enrolment into experiments. Mice that died or had to be humanely euthanized prior to the experimental endpoint (<5% of mice) were excluded from analyses. All mice that reached experimental endpoint were included in the analyses.

Sample Size Calculations

Sample size calculation was carried out using ClinCalc (Kane SP. Statistics. ClinCalc: https://clincalc.com/Statistics. Updated May 21, 2016). For an effect size of 40%, with a SD of 20%,

alpha of 0.05, and power of 0.95, the calculated sample size was n=6 per group.

Bone Marrow Transplantation

Bone marrow (BM) was flushed out of femurs and tibias from 10-week-old male and female PDZK1$^{WT/WT}$LDLR$^{KO/KO}$ and PDZK1$^{KO/KO}$LDLR$^{KO/KO}$ mice with Iscove's Modified Dulbecco's media (Gibco, Thermo Fisher Scientific, Ottawa, ON, Canada) containing 2% FBS, and supplemented with 2 mM L-glutamine, 50 µg/mL penicillin, and 50 U/mL streptomycin as previously described.[56,63] Recipient (10-week-old male or female) PDZK1$^{KO/KO}$LDLR$^{KO/KO}$ mice were exposed to 933 and 467 cGy of 137Cs irradiation using a Gammacell 3000 small animal irradiator (Best Theratronics, Ottawa, ON, Canada), with a 3-hour interval between the two doses. Each pair of potential recipients were randomly put into 2 "bins," assigned to receive either PDZK1$^{WT/WT}$LDLR$^{KO/KO}$ or PDZK1$^{KO/KO}$LDLR$^{KO/KO}$ bone marrow cells (3×106 BM cells injected IV within 2 hours after the second irradiation). After bone marrow transplantation individual mice were assigned codes, mice were allowed to recover for 2 weeks in autoclaved cages with sterile food and water and hydrating gel. After the recovery period, mice were returned to ventilated cages with automatic watering and atherosclerosis was induced as described below. The experimenter was aware of the initial allocation of mice into groups for bone marrow transplantation but was blinded to the identities of the mice after assignment of codes. All analysis were done using this code to avoid bias during analysis and results.

Atherosclerosis Model

For atherosclerosis induction, mice (10 weeks of age or 12 weeks of age for bone marrow transplantation mice, 25–30 g) were fed a HFD (21% butter fat and 0.15% cholesterol, Dyets, Inc, Bethlehem, PA, USA, CAT#112286) for 10 weeks. After that, mice were fasted for 4 hours, followed by euthanasia (CO_2 asphyxiation and cervical dislocation). Blood was collected by cardiac puncture using heparinized 1mL U-100 Insulin Syringe 28G×1/2" MicroFine Needle (BDTM, Mississauga, Canada), and plasma was frozen at −80 °C for subsequent analysis. Mice were perfused with phosphate buffered saline containing 10 U of heparin/mL, and tissues were harvested and fixed in 10% formalin for 48 hours and then embedded in paraffin. Ten serial cross-sections (5 µm thicknesses collected at 100 µm intervals along the aortic sinuses—covering 500 µm in total) were stained with Mayer's hematoxylin and eosin (H&E). Images were captured using a Zeiss Axiovert 200 M inverted microscope (Carl Zeiss Canada Ltd, Toronto, ON, Canada). Total plaque and necrotic core areas were determined by quantitative morphometry using AxioVision 3.1.2.1 software (Carl Zeiss Canada Ltd, Toronto, ON, Canada) and quantified as the sum of the cross-sectional areas of each H&E-stained atherosclerotic plaque in each section. To minimize observer error, images were analyzed in a blinded manner. Atherosclerotic plaque volumes within the 500 µm distance of the aortic sinus were calculated as the area under the curve of cross-sectional area versus distance along the aortic sinus for each mouse.

Plasma Analysis

Enzymatic assay kits were used to measure total cholesterol (Thermo Fisher, Ottawa, ON, Canada), unesterified cholesterol, and HDL-cholesterol (FujiFilm Medical Systems, formerly Wako Diagnostics, Richmond, VA) following the manufacturer's instructions. Cholesteryl ester and non-HDL cholesterol values were determined by subtraction of unesterified cholesterol or HDL-cholesterol (respectively) from total cholesterol.

Immunofluorescence

Immunostaining for Apoa1, Mac-3, phospho-MLKL, and/or phospho-RIPK3 was carried out as described below. For paraffin sections of atherosclerotic plaques in the aortic sinus, one section per mouse, corresponding to the peak atherosclerotic cross-sectional area (see Figures S1H, S1I, S8H, S8I, S9H, S9I) was used. Paraffin sections were deparaffinized as described by others.[64] Deparaffinized sections were incubated with sodium citrate buffer (10 mM sodium citrate, 0.05% tween 20, pH 6.0) for 40 minutes at 95 °C to unmask antigens and epitopes. Then, slides were washed with PBS, two times for 5 minutes. Sections were permeabilized with 0.01% Triton X-100 for 5 minutes at room temperature. Sequential co-immunofluorescence staining was performed as described by others.[65] Briefly, sections were incubated with blocking solution (PBS+5% goat serum), followed by incubation with rabbit anti-phospho MLKL (1:500) antibody in blocking solution at 4 °C overnight. Then slides were washed three times with PBS-T (PBS + 0.01% tween 20), followed by labeling with Alexa 594 goat anti-rabbit (1:200 in PBS-T). Slides were washed three times and sections were blocked again for 1 hour at room temperature, followed by incubation with rabbit anti-phospho RIPK3 (1:500) antibody in blocking solution at 4 °C overnight. Then, sections were labeled with Alexa 488 goat anti-rabbit (1:200 in PBS-T). Sections were counterstained for nuclear DNA with 300 nM 4′,6-diamidino-2-phenylindole (DAPI). Rabbit mAb IgG isotype control (Cell Signaling Technology, Whitby, Ontario, Canada; 1:500) was used as a negative control. The same protocol described above was used to stain a subset of samples for rabbit anti-Apoa1 (1:100 in 5% goat serum) and rat anti-Mac-3 (1:100 in 5% goat serum); rabbit anti-phospho-MLKL (1:500) and Mac-3; rabbit anti-phospho-RIPK3 (1:500) and Mac-3 co-immunostaining. For peritoneal macrophages, cells were fixed in 2.5% fresh paraformaldehyde for 20 minutes at room temperature, followed by permeabilization with 0.01% TritonX-100 for 3 minutes at room temperature. Then, sequential co-immunofluorescence staining protocol was applied in cells. Fluorescent images were captured using a XLAS Stellaris 5 inverted confocal microscope (Leica Microsystems, Inc, Concord, Ontario, Canada). To minimize technical variations, for each experiment, all samples to be compared were stained and imaged at the same time. To minimize observer error, images were analyzed in a blinded manner. Slides were labeled with a code that did not identify the type of treatment or the genotype of mice. For quantification of pRIPK3 or pMLKL staining, the area of positive staining (independent of cell types) within the cross-section of the atherosclerotic plaque was determined using Image J software and was divided by the total area of the atherosclerotic plaque cross-section. For quantification of pRIPK3 and pMLKL staining in cultured cells, 5 fields of

view (20× magnification) were captured and total fluorescence intensity of the 5 fields was determined using Image J software and normalized to the total number of DAPI stained nuclei in the five fields of view.

Culture and Treatment of Peritoneal Macrophages and THP-1 Cells

Mice were injected intraperitoneally on day 0 with 1 mL of sterile 10% thioglycollate. On day 4, mice were euthanized by CO_2 asphyxiation and cervical dislocation. Mouse peritoneal macrophages (MPMs) were collected with ice cold PBS containing 5 mM EDTA. MPMs were washed once in Dulbecco´s Modified Eagle´s Medium (DMEM) containing 20% FBS. Cells were plated (1.5×10^5 cells/well) in 8-well EZ-LINE Chamber Slides (Bio Basic, Inc, Markhan, ON, Canada) and cultured in DMEM containing 2 mM L-glutamine, 50 U/ml penicillin, and 50 mg/ml streptomycin with 10% FBS (complete medium I) overnight.

Human monocyte-like THP-1 cells were cultured in Roswell Park Memorial Institute (RPMI) medium containing 10% FBS supplemented with 2 mM L-glutamine, 50 U/ml penicillin and 50 mg/ml streptomycin (complete medium II). Cells were regularly passaged at subconfluency (≈8×10^5 cells/mL), ensuring their concentration did not exceed 1×10^6 cells/mL. THP-1 monocytes were plated (1.5×10^5 cells/well) in 8-well EZ-LINE Chamber Slides (Bio Basic, Inc, Markhan, ON, Canada) and differentiated into macrophages by 48 hour incubation in complete medium II supplemented with 10 ng/mL phorbol 12-myristate 13-acetate (PMA), followed by 24-hour incubation in complete medium II without PMA. Before each experiment, complete medium I and II were replaced with the corresponding medium containing 3% newborn calf lipoprotein–deficient serum,[66] 2 mM L-glutamine, 50 U/mL penicillin, and 50 mg/mL streptomycin (lipoprotein-deficient medium) and cultured overnight. At the start of each experiment, lipoprotein-deficient medium was replaced with fresh lipoprotein-deficient medium.

Cell Death Analysis

MPMs or THP-1 cells were incubated with 50 µg/mL highly-oxidized LDL (h-oxLDL) or 100 nM TNF (tumor necrosis factor)-α plus 50 µM carbobenzoxy-valyl-alanyl-aspartyl-[O-methyl]-fluoromethylketone (ZVAD), a cell-permeant pan-caspase inhibitor, 50 µg/mL HDL (all lipoprotein concentrations reported in µg protein/mL) or 0.3% DMSO as a vehicle for 24 hours. In other experiments, cells were treated with 10 µM LY294002 (PI3K inhibitor; Cell Signaling Technologies, Inc, Danvers, MA), 3 µM Akt V (pan-AKT inhibitor; Millipore Canada Ltd, Etobicoke, ON, Canada), 100 nM bpV-pic (PTEN inhibitor; Sigma-Aldrich Canada Co. Ottawa, ON, Canada), 12.5 to 800 µM Nec-1s (necroptosis inhibitor; BioVision, Inc, Milpitas, CA). All inhibitors were applied to cells 10 minutes prior to other treatments. Then, cells were stained with 1 µg/mL propidium iodide (PI; Sigma-Aldrich Canada Co. Ottawa, ON, Canada), washed 3X with ice-cold PBS, fixed with 2.5% fresh paraformaldehyde for 20 minutes at room temperature, and counterstained with 300 nM DAPI for 5 minutes at room temperature to identify nuclei. Images were captured using a Zeiss Axiovert 200 M inverted fluorescence microscope (Carl Zeiss Canada, Ltd, Toronto, ON, Canada). Necrotic nuclei were identified as having PI nuclear staining. Necrotic cell numbers were counted across 5 fields of view for each well. Percentage ratios of the numbers of PI-stained/total nuclei for 5 fields were taken as measures of the proportions of necrotic cells per well and were averaged across quadruplicate wells. In some experiments, lactate dehydrogenase released from cells into the cell culture medium was used as an alternate measure of cytotoxicity. At the end of treatments, cell culture medium was collected, subjected to centrifugation to pellet any non-adherent cells/debris, and released LDH was measured using an LDH assay kit (Sigma-Aldrich Canada Co, Ottawa, ON, Canada) following the manufacturer's protocol. For positive control, cells were lysed with lysis buffer provided by the kit. After that, cells and media were centrifuged, and the supernatant was collected and LDH was measured in parallel with other treatments. For negative control, the media from untreated cells was collected, and centrifuged to pellet any nonadherent cells/debris and released LDH was measured.

Immunoblotting Analysis

MPMs were serum starved for 18 hours prior to treatments. Cells were lysed on ice-cold RIPA buffer (50 mM Tris-HCl pH 7.4; 150 mM NaCl; 1% Triton X-100; 1% sodium deoxycholate; 0.1% SDS; 1 mM EDTA) in the presence of protease inhibitors (1 mg/ml pepstatin A; 1 mg/ml leupeptin; 10 mg/ml aprotinin; 50 mM APMSF). For phospho-protein analyses, 1X PhosSTOP phosphatase inhibitor cocktail (Roche, Mannhein, Germany) was included. Protein concentrations in supernatants were determined (BCA assay, Pierce Biotechnology, Rockford, IL), and 50 µg proteins were subjected to SDS-polyacrylamide (10%) gel electrophoresis and immunoblotting on Immobilon-P polyvinylidene difluoride (PVDF) membranes.[67,68] PVDF membranes were blocked (1 hour, room temperature) with 5% bovine serum albumin in TBST (20 mM Tris, 150 mM NaCl, 0.1 % Tween-20), incubated with primary antibodies (4 °C overnight) and secondary antibodies (1.5 hours at room temperature) diluted as indicated, with 5 washes in TBST in between. Primary antibodies were rabbit anti-phospho-Akt (Ser473) mAb (1:500 in 5% BSA), rabbit anti-Akt antibody (1:500 in 5% BSA), rabbit anti-phospho-TAK1 (Thr184, Thr187) mAb (1:500 in 5% BSA), rabbit anti-TAK1 (1:500 in 5% BSA), rabbit anti-phospho-TBK1 (Ser 172) pAb (1:500), rabbit anti-TBK1 (1:500 in 5% BSA), rabbit anti-phospho RIPK3 (Ser 227) mAb (1:500 in 5% BSA), rabbit anti-RIPK3 (1:500 in 5% BSA), rabbit anti-phospho MLKL (Ser 345) mAb (1:500 in 5% BSA), rabbit anti-MLKL (1:500 in 5% BSA). Secondary antibody was HRP-goat anti-rabbit IgG (each 1:5000 in blocking solution). HRP was detected using Pierce ECL Western Blotting Substrate (Thermo Fisher Scientific, Ottawa, ON, Canada), and a Gel Doc instrument (Bio-Rad Laboratories, Hercules, CA). Membranes were stripped and re-probed using HRP-anti-β-actin (1:5000 in blocking solution, overnight) as a control for equal loading.

Real-Time Quantitative Reverse-Transcriptase Polymerase Chain Reaction

MPMs were cultured for 48 hours at 37 °C in DMEM supplemented with 10% FBS. Total RNA was extracted from cells and purified using the RNeasy Mini Kit (Qiagen; cat: 74104) according to the manufacturer's instructions. cDNA was synthesized using the Applied Biosystems High-Capacity cDNA Reverse Transcription Kit (Fisher Scientific; cat: 4368814) according to

the manufacturer's protocol. One thousand nanograms of total RNA was reverse transcribed to cDNA and diluted in ddH2O to a final concentration of 5 ng/μL. Gene expression was measured by real time quantitative reverse-transcriptase polymerase chain reaction with a single reaction (final volume=25 μL) consisting of 25 ng of cDNA, 0.4 μM forward primer, 0.4 μM reverse primer, and 1X SYBR green dye (Invitrogen; cat 11744). Gapdh was detected as an internal control. All primers (Major Resources Table in the Supplemental Material) were synthesized by Invitrogen (Burlington, ON, CA). PCR reactions were loaded on an Applied Biosystems™ MicroAmp Fast Optical 96-Well Reaction Plate (Fisher Scientific; cat: 4246907) and analysed on the StepOnePlus Real Time PCR system and StepOne Software v2.2.2 (Applied Biosystems, Foster City, CA). The following PCR program was used: holding stage (95°C for 10 minutes), cycling stage (40 cycles: denaturation-95°C for 15 seconds; annealing/extension-60°C for 1 minute), melt curve stage (95°C for 15 seconds; 60°C for 1 minutes to 95°C for 15 seconds at a ramp increment of 0.3°C). The relative amount of Pdzk1 mRNA was calculated using the delta-delta Ct method (2−ΔΔCt), where Ct (cycle threshold), is calculated by the StepOne software and corresponds to the PCR cycle number where the fluorescence signal of the reaction is distinguishable from the baseline signal.

Statistical Analysis

All data were assessed for normality (D'Agostino-Pearson test) and equal variance (*F* test) to determine the appropriateness of a subsequent parametric or nonparametric test. For comparison of two groups, those data that passed the afore mentioned tests were analyzed by the unpaired Student *t*-test with Welch correction. Those that did not pass the tests for normality and equal variance (Figure S4) were analyzed by the Mann-Whitney rank sum test. Repeated-measures 2-way ANOVA with Tukey multiple comparisons test was used for weekly weight analysis (Figure S1, S8, S9A, and S9B). Data from multiple groups were analyzed by 1-way or 2-way ANOVA followed by Sidak or Tukey multiple comparisons test to evaluate the statistical significance for comparisons with 1 or 2 independent variables, respectively, using GraphPad Prism (GraphPad Software v.8.0, San Diego, CA). Data are presented as mean±SEM, except for Figure S4, which data are presented as median and 95% CIs. Data were considered statistically significant when $P<0.05$.

RESULTS

Genetic Overexpression or Knockout of ApoA1 Has Opposite Effects on Necrotic Core Development Within Atherosclerotic Plaques in Mice

To investigate the influence of HDL levels on necrotic core development within atherosclerotic plaques, ApoA1$^{KO/KO}$LDLR$^{KO/KO}$, ApoA1$^{WT/WT}$LDLR$^{KO/KO}$, and hApoA1$^{TG/TG}$LDLR$^{KO/KO}$ mice were fed a HFD for 10 weeks. Body weights measured weekly over the course of HFD feeding were similar among the genotypes (Figure S1A and S1B). Consistent with previous reports,[69–72] ApoA1$^{KO/KO}$LDLR$^{KO/KO}$ mice have reduced while hApoA1$^{TG/TG}$LDLR$^{KO/KO}$ mice have substantially increased HDL cholesterol levels compared to control ApoA1$^{WT/WT}$LDLR$^{KO/KO}$ mice (ApoA1$^{KO/KO}$LDLR$^{KO/KO}$; ApoA1$^{WT/WT}$LDLR$^{KO/KO}$; hApoA1$^{TG/TG}$LDLR$^{KO/KO}$ males—8.94±4.72 mg/dL; 20.89±3.82 mg/dL; 36.08±2.72 mg/dL, $P<0.0001$. Females—10.12±1.24 mg/dL; 18.26±2.32 mg/dL; 33.17±2.16 mg/dL, $P<0.0001$ by 1-way ANOVA—Figure S1C). In samples from males, alterations also were observed in non-HDL cholesterol (1240±205.4 mg/dL; 1831±152.3 mg/dL; 2627±85.6 mg/dL; $P<0.0001$ by 1-way ANOVA), total cholesterol (1300±73.8 mg/dL; 2171±102.14 mg/dL; 2813±123.1 mg/dL, $P<0.0001$ by 1-way ANOVA), free cholesterol (547.6±78.21 mg/dL; 814±47.1 mg/dL; 1247.6±75.19 mg/dL, $P<0.0001$ by 1-way ANOVA), and esterified cholesterol (835.5±40.3 mg/dL; 1231±20.5 mg/dL; 1570±25.3 mg/dL, $P<0.0001$ by 1-way ANOVA—Figure S1D through S1G). Similar results were observed in females. Both male and female ApoA1$^{KO/KO}$LDLR$^{KO/KO}$ mice exhibited increased, while hApoA1$^{TG/TG}$LDLR$^{KO/KO}$ mice exhibited reduced atherosclerotic plaque sizes compared to corresponding ApoA1$^{WT/WT}$LDLR$^{KO/KO}$ mice fed the same diet for the same period (males, plaque size—6.12±1.3×10^7 μm^3; 3.8±1.5×10^7 μm^3; 1.3±0.95×10^7 μm^3; $P=0.0002$, 0.0001, 0.0002—females, plaque size—6.3±1.6×10^7 μm^3; 3.3±1.2×10^7 μm^3; 1.5±0.6×10^7 μm^3; $P=0.0001$, 0.0001, 0.0001 by 1-way ANOVA—Figure 1A through 1C; Figure S1H and S1I). Immunofluorescence staining revealed the presence of ApoA1 in regions of atherosclerotic plaques containing macrophages (Mac3$^+$ staining) in samples from ApoA1$^{WT/WT}$LDLR$^{KO/KO}$ mice, increased staining for ApoA1 in macrophage rich areas of plaques from hApoA1$^{TG/TG}$LDLR$^{KO/KO}$ mice, and no detection of ApoA1 in plaques from ApoA1$^{KO/KO}$LDLR$^{KO/KO}$ mice (Figure S2A). Atherosclerotic plaques in male and female ApoA1$^{KO/KO}$LDLR$^{KO/KO}$ mice exhibited substantially larger necrotic cores, while necrotic cores in atherosclerotic plaques of hApoA1$^{TG/TG}$LDLR$^{KO/KO}$ mice were substantially smaller than those from control ApoA1$^{WT/WT}$LDLR$^{KO/KO}$ mice (males—necrotic core—15.7±2.3%; 9.3±1.2 %; 3.26±0.8%, $P=0.0001$, 0.0001, 0.0001; females—necrotic core—16.2±1.7%; 9.5±0.3%; 3.1±0.5%, $P=0.0002$, 0.0001, 0.0001 by 1-way ANOVA—Figure 1D and 1E).

Since necroptosis has been demonstrated to be a driver of necrotic core development in atherosclerotic plaques, we investigated the phosphorylation levels of key mediators of necroptosis, RIPK3 and MLKL, in atherosclerotic plaques from all groups of mice. Immunofluorescence staining revealed abundant staining of phospho-RIPK3 and phospho-MLKL in atherosclerotic plaques from ApoA1$^{KO/KO}$LDLR$^{KO/KO}$ mice (Figure 1F; Figure S3, with negative control antibody staining). Co-immunofluorescence staining of samples from a subset of mice revealed that both phospho-RIPK3 and phospho-MLKL were detected in macrophage rich (Mac3$^+$ staining) regions of plaques (Figure S2B and S2C).

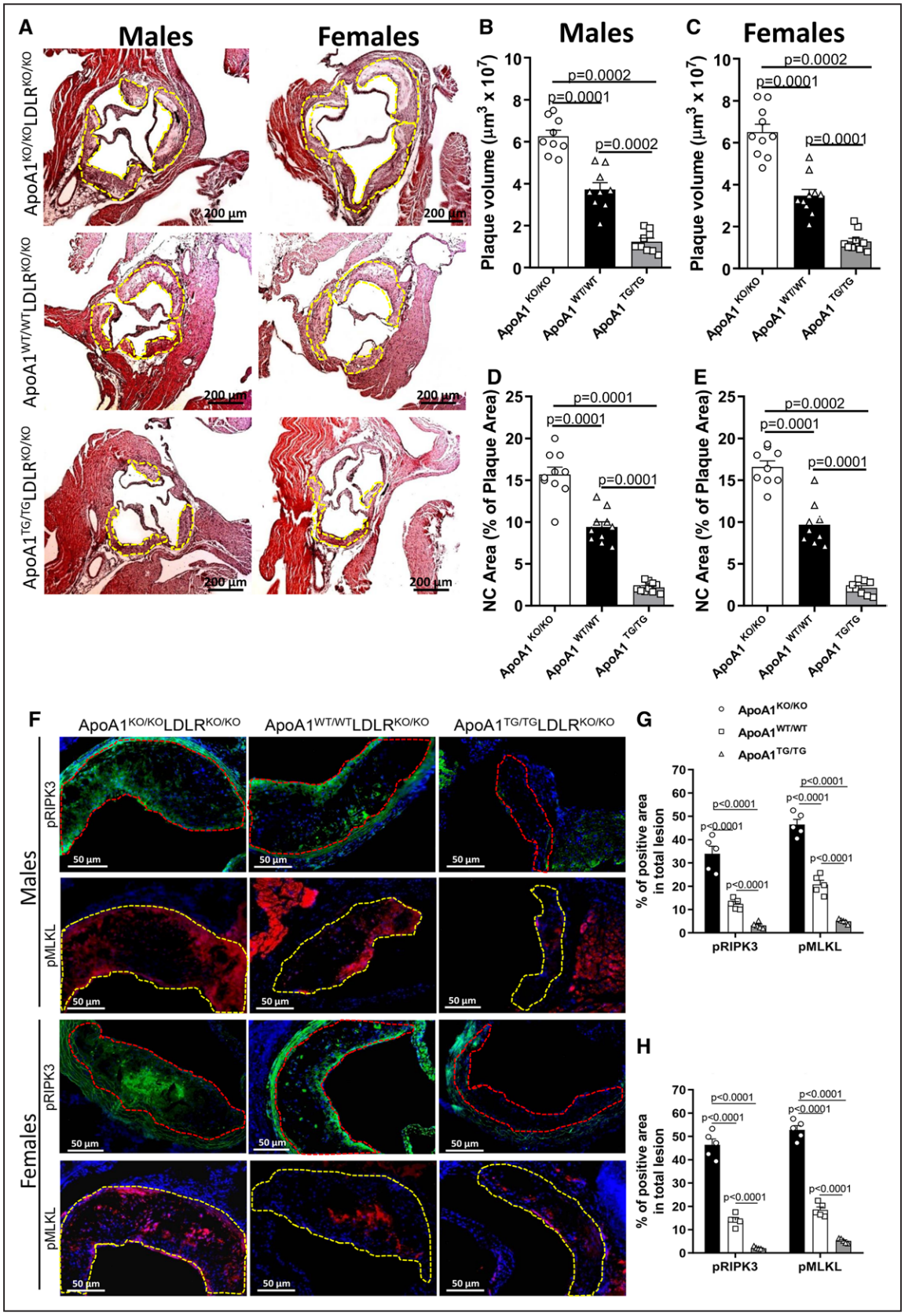

Figure 1. Effects of genetically varying ApoA1 (apolipoprotein A1) levels in low-density lipoprotein receptor (LDLR) KO mice on atherosclerotic plaque and necrotic core sizes and levels of phosphorylated RIPK3 (receptor interacting protein kinase 3) and MLKL (mixed lineage kinase domain-like protein).

Male and female ApoA1$^{WT/WT}$/LDLR$^{KO/KO}$, ApoA1$^{KO/KO}$/LDLR$^{KO/KO}$, or hApoA1$^{TG/TG}$/LDLR$^{KO/KO}$ mice (10-week-old, n=10/group) were challenged with a high-fat diet for 10 weeks. **A**, Representative images of H&E-stained atherosclerotic plaques from ApoA1$^{KO/KO}$LDLR$^{KO/KO}$, (*Continued*)

Immunofluorescence analysis of all cells within atherosclerotic plaque sections of samples were analyzed individually for phospho-RIPK3 or phospho-MLKL and revealed that both male and female ApoA1$^{KO/KO}$LDLR$^{KO/KO}$ mice showed significant increases in levels of phospho-RIPK3 in atherosclerotic plaques when compared to those from ApoA1$^{WT/WT}$LDLR$^{KO/KO}$ and hApoA1$^{TG/TG}$LDLR$^{KO/KO}$ (ApoA1$^{KO/KO}$LDLR$^{KO/KO}$; ApoA1$^{WT/WT}$LDLR$^{KO/KO}$; hApoA1$^{TG/TG}$LDLR$^{KO/KO}$ males—32.1±3.2%; 11.5±1.2%; 2.3±0.4%, $P<0.0001$; females—45.1±2.5%; 17.2±0.8%; 1.2±0.2%, $P<0.0001$ by 1-way ANOVA) and phospho-MLKL (males—48.3±2.3%; 20.3±1.6%; 4.2±0.3%, $P<0.0001$; females—53.2±2.1%; 20±1.3%; 3.9±0.4%, $P<0.0001$ by 1-way ANOVA—Figure 1F and 1H). This suggests that reductions in ApoA1 are associated with activation of necroptosis within atherosclerotic plaques.

HDL Mediates Protection Against Highly Oxidized LDL or TNFα-Induced-Necroptosis in Macrophages

To determine if HDL was able to directly protect macrophages against necroptosis, we treated MPMs in culture with h-oxLDL in the presence of a pan-caspase inhibitor, ZVAD, following conditions reported previously to induce necroptosis.[14] Cellular necrosis was measured by PI staining in unfixed cells. Treatment with h-oxLDL+ZVAD resulted in increased PI staining of macrophage nuclei compared to that of untreated macrophages (24.05±2.3 % PI$^+$ versus 3.1±1.2 % PI$^+$, $P<0.0001$, Figure 2A and 2B). This was inhibited by increasing concentrations of the RIPK1 inhibitor Nec-1s (Figure 2A and 2B), confirming that it represented necroptosis.[73] Similarly, h-oxLDL+ZVAD-induced PI staining was reduced when cells were treated with increasing concentrations of HDL with maximal inhibition at approximately 50 µg (HDL protein)/mL (Figure 2C). The extent of inhibition of PI staining with HDL was comparable to the maximal inhibition observed with Nec-1s. Treatment of MPMs with TNFα+ZVAD for 24 hours also resulted in a similar increase in PI staining of macrophage nuclei which was substantially reduced in the presence of HDL (50 µg protein/mL; 37±2.3 % PI$^+$ versus 18±1.1% PI$^+$, $P=0.002$, Figure 2D and 2E). In contrast, only minimal Annexin V staining was observed (Figure 2F and 2G), indicating that treatment with TNFα+ZVAD did not trigger apoptosis. Pre-treatment of cells with HDL for 24h, resulted in a similar suppression of TNFα+ZVAD-induced cell death as measured by PI staining (no HDL: 43±1.5 % PI$^+$ versus HDL: 21±2.3 % PI$^+$, $P<0.0001$, Figure 2H and 2I).

HDL Protection Against Necroptosis in Macrophages Requires SR-B1, PDZK1, and the PI3K/Akt Signaling Pathway

To examine the involvement of the HDL receptor, SR-B1, and the adaptor protein, PDZK1 in HDL-mediated protection of macrophages against necroptosis, MPMs from wild type (WT), SR-B1$^{KO/KO}$ (lacking SR-B1 expression), SR-B1$^{deltaCT/deltaCT}$ (expressing a truncated mutant form of SR-B1, lacking the carboxy-terminal amino acids that interact with the adaptor protein, PDZK1), and PDZK1$^{KO/KO}$ mice (lacking expression of PDZK1; see Figure S3) were treated with TNFα+ZVAD in the presence or absence of HDL. Analysis of cytotoxicity using an LDH-release assay confirmed that treatment of macrophages from WT mice with TNFα+ZVAD triggered cytotoxicity, which was attenuated when HDL was present (42±1.2% versus 21±3.4% cytotoxicity, $P<0.001$, Figure 2J). Similarly, treatment of macrophages from SR-B1$^{KO/KO}$, SR-B1$^{deltaCT/deltaCT}$ or PDZK1$^{KO/KO}$ mice with TNFα+ZVAD triggered cytotoxicity; however, this was not attenuated by HDL (SR-B1$^{deltaCT/deltaCT}$, 45±4% versus 53±2.1%; SR-B1$^{KO/KO}$, 56±1.2% versus 50±2.3%; PDZK1$^{KO/KO}$, 48±1.5 versus 45±2.6% cytotoxicity, Figure 2J through 2M). Similar results were observed when macrophages from WT, SR-B1$^{KO/KO}$ and PDZK1$^{KO/KO}$ mice were treated with oxLDL+ZVAD in the absence or presence of HDL and PI nuclear staining was measured (Figure S5A and S5B).

Treatment of MPMs from WT mice with HDL in the presence of TNFα+ZVAD resulted in a significant increase in the level of phospho-Akt (2.1±0.1 relative units, ru), phospho-TAK1 (3.2±0.3 ru), and phospho-TBK1 (2.5±0.3 ru) whereas macrophages treated with TNFα+ZVAD alone exhibited reduced Akt, TAK1, and TBK1 phosphorylation (0.25±0.1; 0.9±0.1; 1.2±0.2 ru, respectively) when compared to control treated macrophages (Figure 3A through 3D). Treatment of MPMs with TNFα+ZVAD and the Akt inhibitor Akt inhibitor V reduced the level of Akt, TAK1, and TBK1phosphorylation (0.2±0.01; 0.5±0.1; 1±0.2 ru, respectively) compared to macrophages treated with TNFα+ZVAD+HDL and prevented HDL-mediated induction of Akt phosphorylation in the presence of TNFα+ZVAD (Figure 3A through 3D). In contrast, the PTEN inhibitor, bpV-pic, resulted in a substantial increase in phospho-Akt,

Figure 1 Continued. ApoA1$^{WT/WT}$LDLR$^{KO/KO}$, and hApoA1$^{TG/TG}$LDLR$^{KO/KO}$ males and females. **B** and **C**, Quantification of plaque volume for males and females. **D** and **E**, Quantification of necrotic core area for males and females. **F**, Representative images of phospho-RIPK3 (green), phospho-MLKL (red), and DAPI (blue)-stained atherosclerotic plaques of male (top 2 rows) and female (bottom 2 rows) ApoA1$^{KO/KO}$LDLR$^{KO/KO}$ (left column), ApoA1$^{WT/WT}$LDLR$^{KO/KO}$ (middle column), and hApoA1$^{TG/TG}$LDLR$^{KO/KO}$ (right column). Yellow dashed lines mark atherosclerotic plaques. **G** and **H**, Quantification of phosphorylation levels of RIPK3 and MLKL in males and females (n=5 mice/group). Data represent mean±SEM, n=5–10 biological replicates. **B** through **E**, Statistical analysis was done using 1-way ANOVA followed by Sidak multiple comparisons test. **G** and **H**, Statistical analysis was done using 2-way ANOVA followed by Tukey multiple comparisons test.

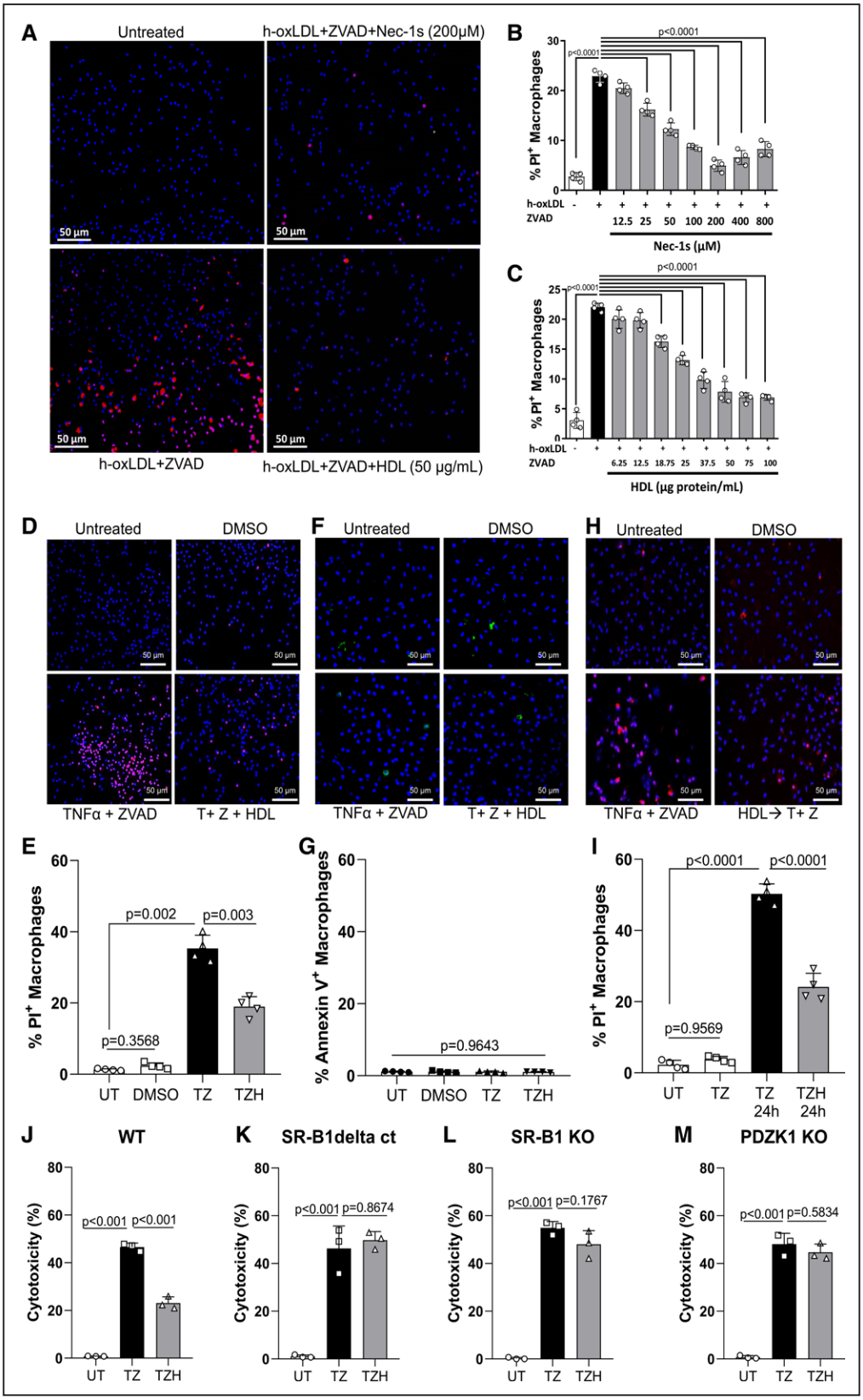

Figure 2. HDL (high-density lipoprotein) mediates protection of cultured peritoneal macrophages against TNFα (tumor necrosis factor alpha) and h-oxLDL (highly-oxidized low-density lipoprotein)-induced necroptosis and requires SR-B1 (scavenger receptor class B type 1), and the adapter protein PDZK1 (postsynaptic density protein/Drosophila disc-large protein/Zonula occludens protein containing 1).

Thioglycollate-elicited peritoneal macrophages were prepared from wild-type (WT), SR-B1 KO, and PDZK1 KO mice and treated as indicated in culture. **A–C**, Cells were cultured in lipoprotein-deficient medium and treated with h-oxLDL (50μg/mL) and ZVAD (50 μM), (*Continued*)

phospho-TAK1, and phospho-TBK1 levels in macrophages treated with TNFα+ZVAD (4.1±0.2; 2.2±0.2; 2.5±0.1 ru, respectively), similar to HDL treatment. The combination of HDL and bpV-pic, however, did not increase phospho-Akt, TAK1, and TBK1 levels further in TNFα+ZVAD-treated macrophages (Figure 3A through 3D). On the other hand, treatment of macrophages with HDL in the presence of TNFα+ZVAD resulted in a significant decrease of phosphorylation levels of RIPK3 and MLKL, when compared with macrophages treated only with TNFα+ZVAD (pRIPK3 0.2±0.1, pMLKL 0.7±0.1 versus pRIPK3 2.5±0.3, pMLKL 2.7±0.2 ru, respectively; Figure 3A, 3E, 3F). Similar results were observed when immunofluorescence staining was used to detect pRIPK3 and pMLKL in similarly treated wild type macrophages (Figure S6A through S6C). Inhibition of Akt with Akt inhibitor V prevented HDL-mediated suppression of RIPK3 and MLKL phosphorylation in TNFα+ZVAD treated wild type macrophages (Figure 3A, 3E, 3F, compare TZ/TZH with TZA/TZAH). Similar results were observed when phosphorylation levels of RIPK3 and MLKL were detected by immunofluorescence in macrophages from wild type mice (Figure S6A through S6C). Likewise, treatment of cells with the PI3K inhibitor LY294002 also impaired the ability of HDL to reduce levels of pRIPK3 and pMLKL in TNFα+ZVAD treated wild type macrophages as detected by immunofluorescence staining (Figure S6A through S6C).

To confirm the involvement of Akt/PI3K pathway in HDL-induced protection against TNFα+ZVAD-induced necroptosis, MPMs from WT mice were treated with TNFα+ZVAD+HDL in the presence or absence of inhibitors for PI3K, Akt, or PTEN. Both PI3K and Akt inhibitors prevented HDL mediated protection against TNFα+ZVAD-induced necroptosis measured by PI staining (40.6±3.6% PI^+ versus 24.3±4.2% PI^+, P=0.00136; 45.2±7.3% PI^+ versus 24.3±4.2% PI^+, P=0.00181, respectively), whereas treatment with PTEN inhibitor alone was sufficient to protect against TNFα+ZVAD induced necroptosis to an extent similar to that of HDL (22.5±5.1 % PI^+ versus 24.3±4.2 % PI^+, respectively, Figure 3G and 3H). Similar results were seen in THP-1 macrophages and peritoneal macrophages treated with h-oxLDL+ZVAD (Figure S5C through S5H). In contrast to wild type cells, HDL was not able to trigger increases in phosphorylation of Akt, TAK1 and TBK1, or suppress phosphorylation of RIPK3 and MLKL in TNFα+ZVAD-treated SR-B1$^{KO/KO}$, SR-B1$^{deltaCT/deltaCT}$, or PDZK1$^{KO/KO}$ macrophages (Figures S6D through S6F, S7A through S7F) or to protect against TNFα+ZVAD-induced necroptosis in macrophages containing the SR-B1$^{deltaCT/deltaCT}$ mutation (Figure S5I through S5K). These results demonstrate that SR-B1, PDZK1, and the PI3K/Akt pathway are necessary for HDL's ability to suppress TNFα+ZVAD-induced phosphorylation of RIPK3 and MLKL and cell death in MPM in culture.

PDKZ1 Regulates Atherosclerotic Plaque Size, Necrotic Core Area and Phosphorylation Levels of MLKL

Next, we investigated the role of PDZK1 in atherosclerotic plaque and necrotic core development. Male and female PDZK$^{WT/WT}$LDLR$^{KO/KO}$ and PDZK1$^{KO/KO}$LDLR$^{KO/KO}$ mice were challenged with HFD for 10 weeks. Weekly weight measurements showed no differences between PDZK1$^{WT/WT}$LDLR$^{KO/KO}$ and PDZK1$^{KO/KO}$LDLR$^{KO/KO}$ in both males and females (Figure S8A and S8B). Consistent with previous reports in mice lacking both PDZK1 and apolipoprotein E,[59] plasma total cholesterol, HDL cholesterol, non-HDL cholesterol, and plasma cholesteryl ester levels were not statistically significantly different whereas plasma free cholesterol levels were slightly increased in both male and female PDZK1$^{KO/KO}$LDLR$^{KO/KO}$ compared to PDZK1$^{WT/WT}$LDLR$^{KO/KO}$ mice (males, 580±50 mg/dL versus 375±55 mg/dL, P=0.015; females, 420±40 mg/dL versus 250±30 mg/dL, P=0.008, Figure S8C through S8G).

Both male and female PDZK1$^{KO/KO}$LDLR$^{KO/KO}$ mice developed increased atherosclerosis compared to PDZK1$^{WT/WT}$LDLR$^{KO/KO}$ mice (males–5.8±0.6×10^7 μm^3; 3.7±0.7×10^7 μm^3; P<0.0001 by unpaired Student t

Figure 2 Continued. Nec-1s (12.5–800 μM), HDL (6.25–100 μg protein/mL; gray bars) or DMSO as a vehicle (control-black bars) for 24 hours. **A**, Representative images of nuclei from necrotic macrophages detected by propidium iodide (PI) staining (red) before fixation; nuclei were counterstained with DAPI (blue) after fixation. **B** and **C**, Quantification of the percentage of PI positive macrophage nuclei after 24-hour treatment in culture with different concentrations of Nec-1s or HDL, respectively. Data are means±SEM, n=4 biological replicates (cells isolated from different mice). Cells were cultured in lipoprotein-deficient medium and treated with TNFα (100 nM), and ZVAD (50 μM), with or without HDL (50 μg protein/mL) or DMSO as a vehicle (control) for 24 hours. Representative images (**D**) and quantification (**E**) of propidium iodide. Representative images (**F**) and quantification (**G**) of FITC-Annexin V-stained cells. Data are means±SEM, n=4 biological replicates (cells isolated from different mice). **F**, Cells were cultured in lipoprotein-deficient medium and treated for 24 hours with HDL (50 μg protein/mL). Then, cells were washed with PBS and media was replaced without HDL. Cells were treated with TNFα (100 nM) and ZVAD (50 μM) or DMSO as a vehicle (control), and harvested 6, 9, and 24 hours after treatment and stained with PI, fixed and then stained with DAPI. **H**, Representative images and quantification (**I**) of propidium iodide after 24 hours of treatment. Data are means±SEM, n=4 biological replicates (cells isolated from different mice). (J-M) Peritoneal macrophages from WT, SR-B1 KO, SR-B1 deltaCT, and PDZK1 KO were treated with TNFα (100 nM), ZVAD (50 μM), in the presence or absence of HDL (50 μg protein/mL) for 24 hours. After treatment, the supernatant from cells were subjected to the LDH assay to evaluate cytotoxicity, following the manufacture's protocol. Graphics shows the percentage of cytotoxicity. Data are means±SEM, n=4 biological replicates (cells isolated from different mice). Statistical analysis was done using 1-way ANOVA followed by Sidak multiple comparisons test.

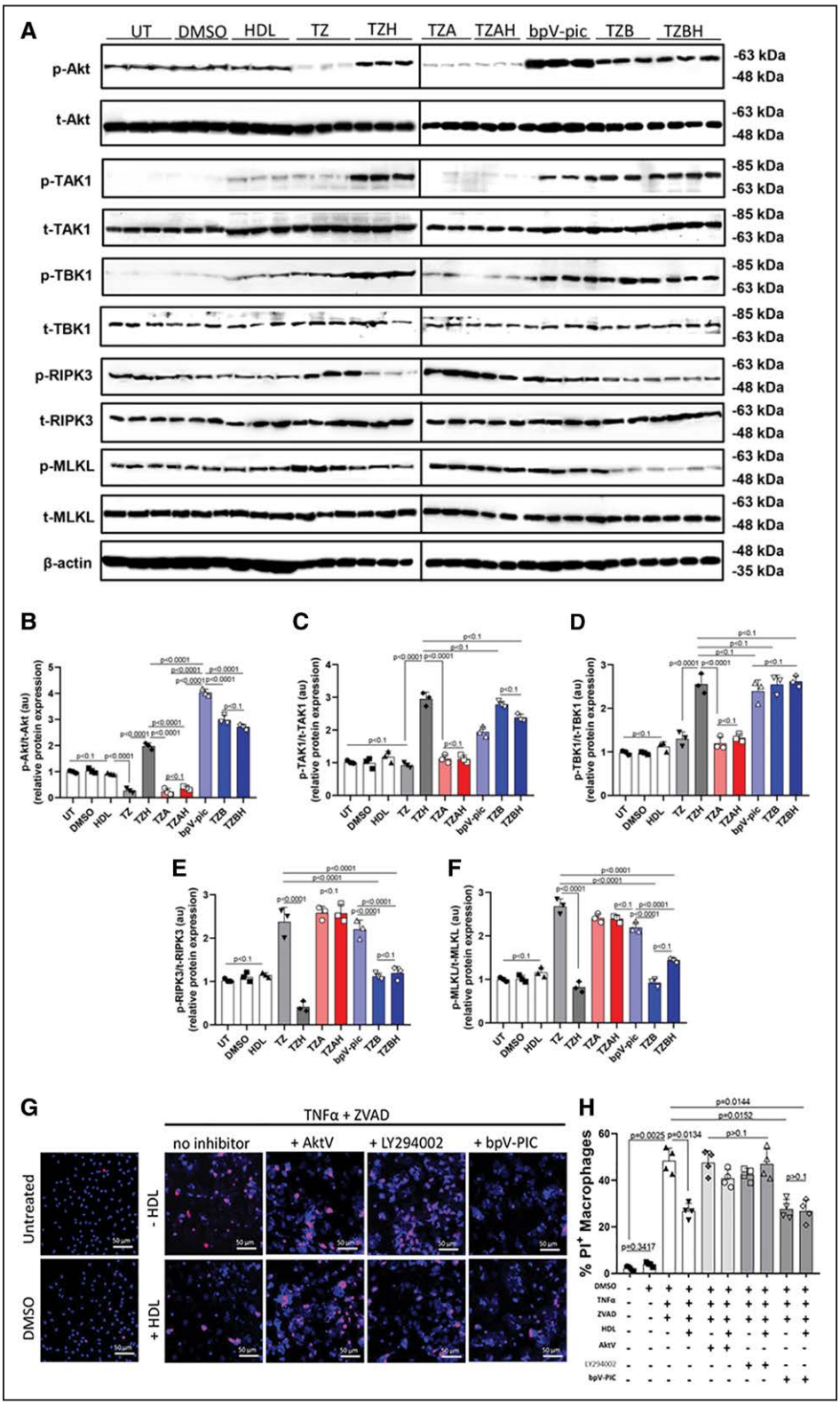

Figure 3. HDL (high-density lipoprotein) protection against TNFα (tumor necrosis factor alpha)-induced necroptosis in macrophages involves activation of the PI3K (phosphoinositide 3-kinase)/Akt pathway. Thioglycollate-elicited peritoneal macrophages prepared from wild-type (WT) mice and cultured in lipoprotein-deficient medium were treated for 24 hours with TNFα (100 nM), ZVAD (50 μM), in the presence or absence of HDL (50 μg protein/mL) and the inhibitors AktV (3 μM), bpV-pic (100 nM), or DMSO as a vehicle (control). Cells were lysed and subjected to SDS-PAGE for immunoblotting. **A**, Representative immunoblots of phospho and total Akt, TAK1 (transforming growth factor beta-activated kinase 1), TBK1 (TANK-binding kinase 1), RIPK3 (receptor interacting protein kinase 3), MLKL (mixed lineage kinase domain-like protein), and β actin. **B**–**F**, Quantification of the ratios of phospho-/total-Akt (**B**), -TAK1 (**C**), -TBK1 (**D**), -RIPK3 (**E**), -MLKL (**F**) band intensities. Quantification was done as relative to UT group (*Continued*)

test—Figure 4A and 4B; females—5.9±0.4×10^7 μm^3; 3.5±0.4×10^7 μm^3; P<0.0001 by unpaired Student t test, Figure 4A through 4C; Figure S8H and S8I), consistent with the increased atherosclerosis reported previously in atherogenic diet fed PDZK1$^{KO/KO}$ApoE$^{KO/KO}$ compared to PDZK1$^{WT/WT}$ApoE$^{KO/KO}$ mice.[59,74] PDZK1$^{KO/KO}$LDLR$^{KO/KO}$ mice also developed larger sized necrotic cores compared to PDZK1$^{WT/WT}$LDLR$^{KO/KO}$ mice (males—18.1±0.5%; 7.2±0.3%; P<0.0001 by unpaired Student t test; females—22.3±0.25%; 8.1±0.5%; P<0.0001 by unpaired Student t test, Figure 4D and 4E). Likewise, the phosphorylation levels of MLKL were higher in the atherosclerotic plaques of PDZK1$^{KO/KO}$LDLR$^{KO/KO}$ compared to PDZK1$^{WT/WT}$LDLR$^{KO/KO}$ mice for both male and female mice (males—58.3±2.1%; 35.2±2.4%; P=0.0004 by unpaired Student t test; females—63.4±2.5%; 41.4±2.7%; P=0.0006 by unpaired Student t test, Figure 4F and 4G).

PDZK1 in BM-Derived Cells Affects Atherosclerotic Plaque Volume and Necrotic Core Size As Well As Key Enzymes Involved in Necroptosis

To determine the extent to which PDZK1 in leukocytes influenced the development of atherosclerotic plaques, necrotic core sizes, and levels of phosphorylated RIPK3 and MLKL within atherosclerotic plaques, we transplanted BM from PDZK1$^{WT/WT}$LDLR$^{KO/KO}$ mice into PDZK1$^{KO/KO}$LDLR$^{KO/KO}$ recipients to restore normal levels of PDZK1 in leukocytes. As controls, we transplanted BM from PDZK1$^{KO/KO}$LDLR$^{KO/KO}$ donors into PDZK1$^{KO/KO}$LDLR$^{KO/KO}$ recipients. Both male and female mice were analyzed. Once the mice recovered from the BM transplantation, atherosclerosis was induced by feeding the BM transplanted mice HFD for 10 weeks. Restoration of the normal WT PDZK1 gene in leukocytes did not affect body weights determined weekly or fasting plasma lipid levels determined at the end of the HFD feeding period (Figure S9A through S9G). However, restoration of the normal WT PDZK1 gene in leukocytes in PDZK1$^{KO/KO}$LDLR$^{KO/KO}$ mice resulted in substantial reductions (about half) in average atherosclerotic plaque and necrotic core sizes in the aortic sinuses for male and female mice (plaque size males—4.7±2.1×10^7 μm^3; 2.6±1.1×10^7 μm^3; P<0.0001; females—4.9±0.9×10^7 μm^3; 2.4±1.7×10^7 μm^3; P<0.0001; necrotic core males—22.3±2.3 %; 11.2±1.6 %; P<0.0001; females—20.4±2.1 %; 12.1±2.2 %; P<0.0001, Figure 5A through 5E; Figure S9H and S9I). Similar decreases were observed in the phosphorylation levels for MLKL and RIPK3 in both male and female PDZK1$^{KO/KO}$LDLR$^{KO/KO}$ mice transplanted with PDZK1$^{WT/WT}$LDLR$^{KO/KO}$ compared to those transplanted with PDZK1$^{KO/KO}$LDLR$^{KO/KO}$ donor bone marrow (Figure 5F through 5K). Together, these results suggest that PDZK1 in leukocytes plays an important protective role counteracting atherosclerotic plaque and necrotic core development, at least in part by attenuating induction of necroptosis.

DISCUSSION

In this study, we demonstrated that eliminating expression of ApoA1 increases atherosclerosis, levels of phosphorylated RIPK3 and MLKL, key mediators of necroptosis, and necrotic core development. On the other hand, overexpressing human ApoA1 reduces atherosclerosis, phosphorylation of RIPK3 and MLKL and necrotic core development within the plaques in both male and female low-density lipoprotein receptor KO mice fed atherogenic HFD.[69,70,72] As reported by others, ApoA1$^{KO/KO}$ mice (also lacking low-density lipoprotein receptor or ApoE expression) fed HFD exhibit reductions in cholesterol associated with both HDL (as expected) and non-HDL lipoproteins.[75,76] Likewise, overexpression of hApoA1 in the LDLR$^{KO/KO}$ mice fed the HFD exhibited the expected increases in HDL cholesterol as well as increases in non-HDL cholesterol similar to effects reported by others.[76–78] To explore one potential pathway by which altering ApoA1 levels modulated necroptosis markers and necrotic core development in atherosclerotic plaques, we examined the effects of HDL on the sensitivity of cultured macrophages to necroptosis.

We have demonstrated that treatment of macrophages (both mouse peritoneal and PMA-differentiated human THP-1 cells) with HDL suppresses necrotic cell death induced by either TNF-α or h-oxLDL (each in the presence of the pan-caspase inhibitor ZVAD). The ability to inhibit this phenomenon with Nec-1s and the induction of phospo-RIPK3 and phospho-MLKL suggest that this represents necroptosis, a programmed form of necrosis that has been implicated in contributing to atherosclerotic necrotic core formation.[14] In cultured cells, HDL-mediated suppression of macrophage necroptosis is dependent on the HDL receptor SR-B1 and the adaptor protein PDZK1 that binds to SR-B1's cytoplasmic C terminus and has been

Figure 3 Continued. (mean±SEM, n=3, biological replicates consisting of cells isolated from different mice). UT (untreated), TZ (TNFα+ZVAD), TZH (TNFα+ZVAD+HDL), TZA (TNFα+ZVAD+AktV), TZAH (TNFα+ZVAD+AktV+HDL), TZB (TNFα+ZVAD+bpV-PIC), TZBH (TNFα+ZVAD+bpV-PIC+HDL). **G** and **H**, Cells were cultured in lipoprotein-deficient medium and treated for 24 hours with TNFα (100 nM) and ZVAD (50 μM), in the absence or presence of HDL (50 μg protein/mL) and the inhibitors AktV (3 μM), LY294002 (10 μM), bpV-pic (100 nM), or DMSO as a vehicle (control). Cells were then stained with PI, fixed and stained with DAPI. **G**, Representative images and (**H**) quantification of cell death as the percentage of PI positive macrophage nuclei. Data are means±SEM, n=4, biological replicates consisting of cells isolated from different mice. Statistical analysis was done using 1-way ANOVA followed by Sidak multiple comparisons test.

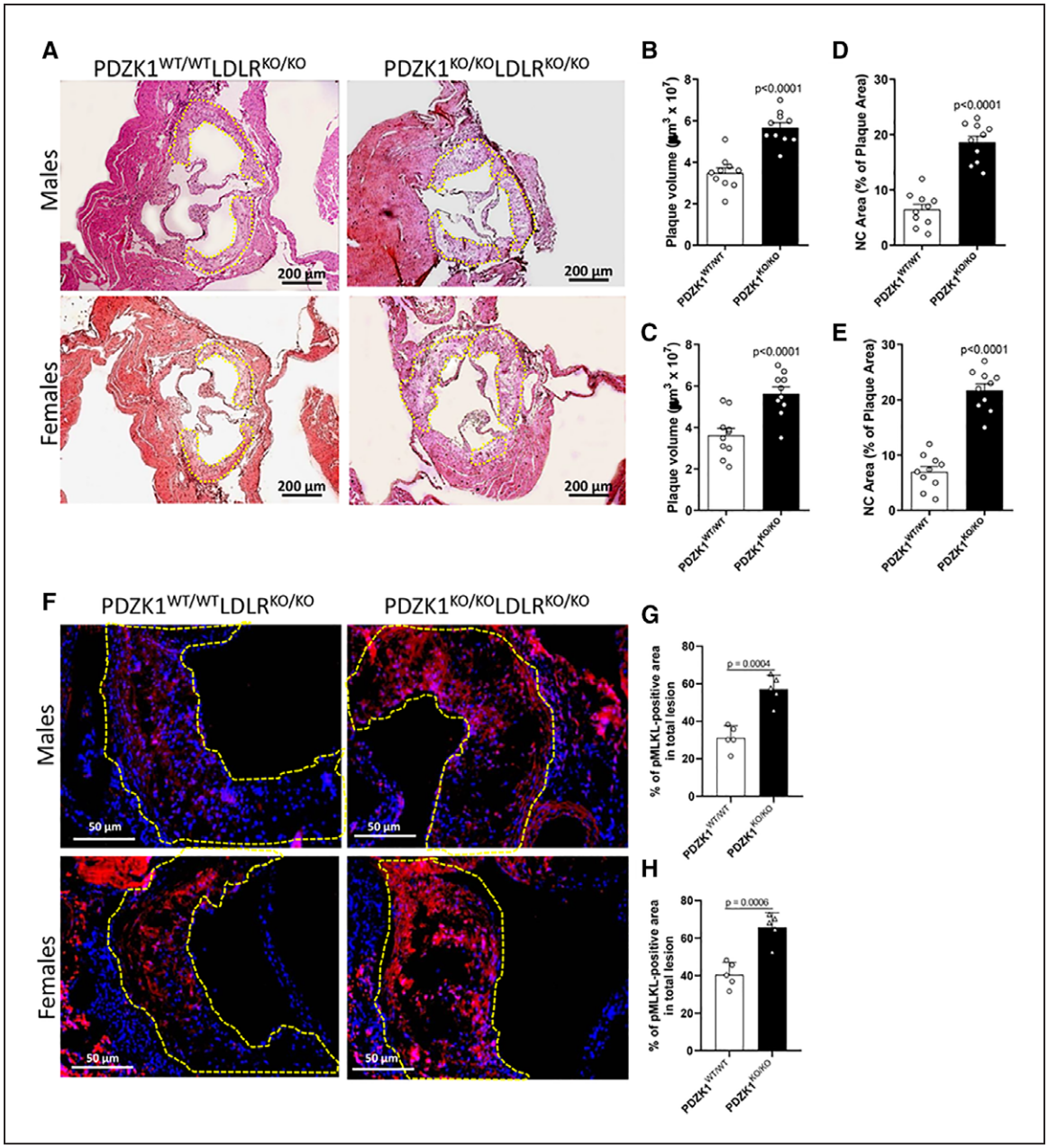

Figure 4. The absence of PDZK1 (postsynaptic density protein/Drosophila disc-large protein/Zonula occludens protein containing 1) increases atherosclerotic lesion and necrotic core area, as well as the phosphorylation levels of MLKL (mixed lineage kinase domain-like protein) in atherosclerotic plaques.

Male and female PDZK1$^{WT/WT}$/LDLR$^{KO/KO}$ and PDZK1$^{KO/KO}$/LDLR$^{KO/KO}$ mice (10-week-old, n=10/group) were fed the atherogenic HFD for 10 weeks. **A**, Representative images of H&E-stained aortic sinus atherosclerotic plaques from males and females. Quantification of (**B** and **C**) plaque volume and (**D** and **E**) necrotic core area for males and females. **F**, Representative images of phospho-MLKL (red) and DAPI (blue)-stained atherosclerotic plaques from PDZK1$^{WT/WT}$/LDLR$^{KO/KO}$ and PDZK1$^{KO/KO}$/LDLR$^{KO/KO}$ males and females. Yellow dashed lines mark atherosclerotic plaques. **G** and **H**, Quantification of pMLKL immunofluorescence in atherosclerotic plaques in males and females, respectively. n=5 biological replicates (individual mice) per group. Data were first subjected to the D'Agostino-Pearson test for normality and for equal variances. Statistical analysis was done using unpaired Student *t*-test. Data are means±SEM.

implicated in SR-B1-dependent HDL-signaling in macrophages and endothelial cells.[79–81] In vivo, either homozygous ApoA1 or PDZK1 KO mutations in low-density lipoprotein receptor KO mice results in increased HFD-induced atherosclerotic plaque and necrotic core development and increased levels of phosphorylated RIPK3 and/or MLKL within plaques. Conversely, restoration of the normal PDZK1 gene in leukocytes of PDZK1$^{KO/KO}$LDLR$^{KO/KO}$ mice reduces levels of phospho-RIPK3 and phospho-MLKL in atherosclerotic plaques and HFD-induced atherosclerosis and necrotic core development. We also demonstrated that HDL treatment resulted in increased Akt phosphorylation in macrophages that were treated with TNFα and ZVAD, and that inhibition of Akt

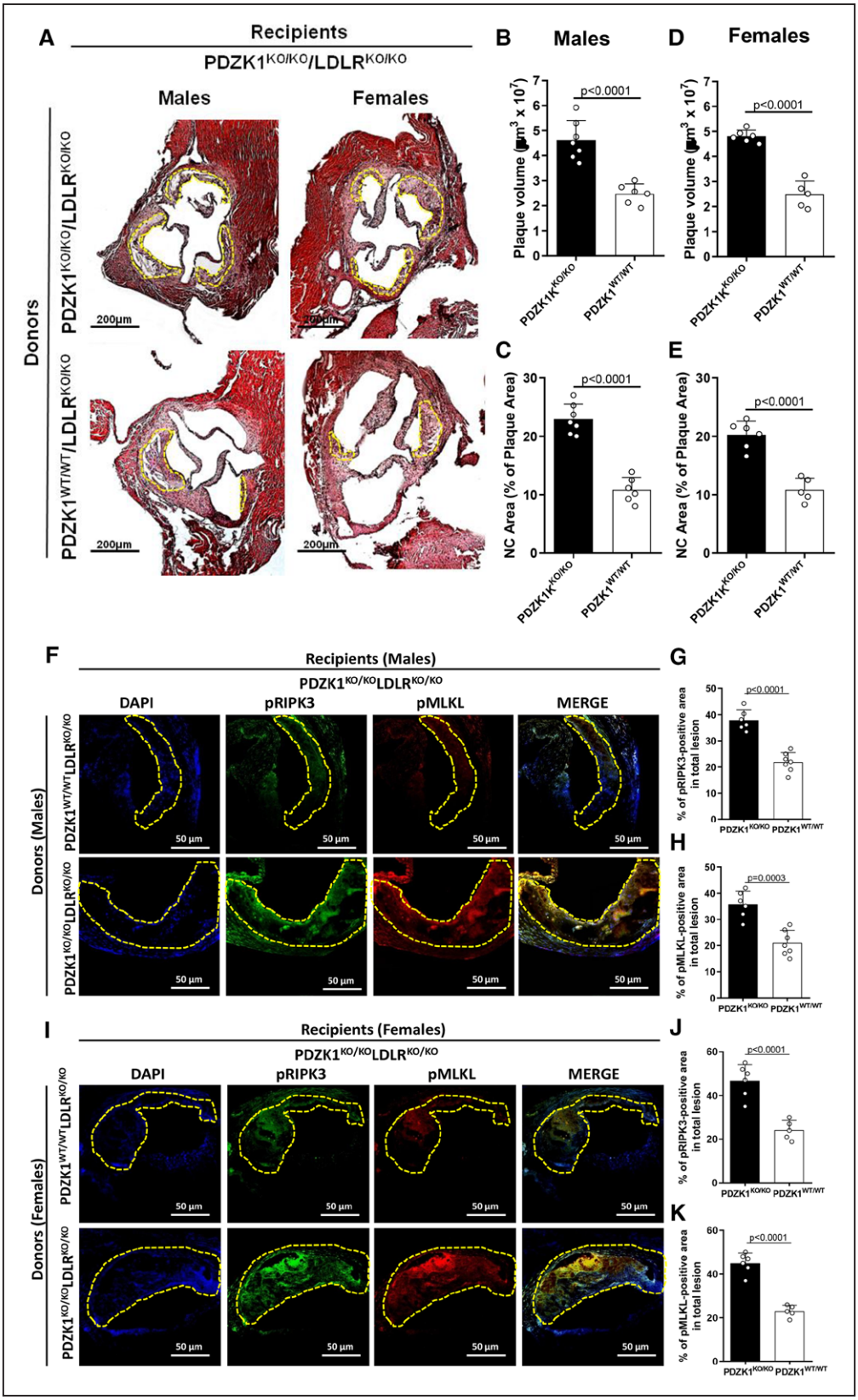

Figure 5. Restoring PDZK1 (postsynaptic density protein/Drosophila disc-large protein/Zonula occludens protein containing 1) in BM-derived cells decreases atherosclerotic lesion and necrotic core areas, and phosphorylation levels of MLKL (mixed lineage kinase domain-like protein) and RIPK3 (receptor interacting protein kinase 3) in atherosclerotic plaques of PDZK1$^{KO/KO}$LDLR$^{KO/KO}$ mice.

Male and female (10-week-old, n=6–7/group) PDZK1$^{KO/KO}$LDLR$^{KO/KO}$ transplanted with PDZK1$^{WT/WT}$LDLR$^{KO/KO}$ or (*Continued*)

phosphorylation abrogated HDL-dependent protection of macrophages from TNFα+ZVAD-induced necroptosis. On the other hand, treatment with the PTEN inhibitor, bpV-pic increased levels of phospho-Akt in macrophages treated with TNFα+ZVAD and this was sufficient to protect them against necroptosis. In bpV-pic-treated cells, HDL treatment resulted in no further increase in either Akt phosphorylation or protection against necroptosis. Together, this suggests that HDL triggers protection against necroptosis through activation of Akt.

HDL has been reported to induce Akt activation in a variety of cell types.[82–84] Our group previously reported that HDL stimulated macrophage migration via a pathway involving Akt1 phosphorylation.[62] We also showed the protection of cardiomyocytes against necrosis induced by oxygen and glucose deprivation through HDL, SR-B1, and PI3K/Akt1/2[85] and the role of HDL-mediated Akt1 activation in the protection against apoptosis in macrophages.[56] Similarly, others have reported HDL signaling in endothelial cells, leading to Akt activation.[61,86,87] However, to our knowledge, this is the first evidence of a role for HDL and Akt phosphorylation in the protection of macrophages against necroptosis.

RIPK1 is an intracellular adaptor protein that relays signals to regulate inflammation, apoptosis, and necroptosis.[88–91] RIPK1 is subject to posttranslational modifications, including ubiquitination and phosphorylation of the kinase domain, and oligomerization via interaction with the RIP homotypic interaction motif (RHIM).[92,93] The activation of RIPK1 is necessary for the formation of the necrosome complex involved in regulation of necroptosis.[92,94] RIPK3, a component of the necrosome complex is phosphorylated by RIPK1 on Ser227, and in turn phosphorylates MLKL on the activation segment residues Thr357/Ser358.[95] The activation of RIPK1 is inhibited by direct phosphorylation by TAK1 (transforming growth factor beta-activated kinase 1), TANK-binding kinase 1 (TBK1), IKKα/β (inhibitor of nuclear factor kappa-β kinase subunit alpha and beta), and MK2 (MAPK-activated protein kinase 2).[96–101] The PI3K/Akt pathway has been shown to be involved in IKKα/β-induced expression of genes involved in cell survival[102–105] and suppressing apoptosis.[103,106] Consistent with evidence that Akt may regulate TAK1,[107] we found that HDL treatment of TNFa+ZVAD-treated WT macrophages was able to induce TAK1 and TBK1 activation along with reducing the activation of RIPK3 and MLKL. The presence of an Akt inhibitor prevented, whereas the presence of PTEN inhibitor promoted TAK1 and TBK1 activation, suggesting that the Akt activation triggered by HDL signaling is involved in the activation of TAK1 and TBK1, key enzymes associated with the regulation of necroptotic cell death. Given our finding that Akt activation or inhibition was associated with reduced or increased levels of induction of RIPK3 phosphorylation, and that RIPK3 is a target for RIPK1 in the induction of necroptosis, our results suggest that Akt activation may interfere directly with the inactivation of RIPK1 through activation of TAK1 and TBK1 to suppress necroptosis.

MLKL activation reportedly requires not only RIPK3-dependent phosphorylation but also binding of highly phosphorylated inositol phosphates (IPs) to its N-terminal domain.[108] Different IP species could exert combinatorial control over MLKL activity by competing for binding sites or influencing other contacts.[108] For example, IP_4, IP_5, and IP_6 are essential for necroptotic induction by human MLKL and implicate the IPPK (inositol pentakisphosphate 2-kinase) enzyme as a significant contributor to MLKL activation through production of IP_6. Nevertheless, the IP code alone cannot activate MLKL and additional activation by RIPK3-mediated phosphorylation is required.[109] As we demonstrated in this study, increased phosphorylation of Akt is associated with decreased phosphorylation of both RIPK3 and MLKL and reduced necroptosis in macrophages, suggesting that the primary mechanism by which HDL stimulation attenuates necroptosis may be via attenuating RIPK3-mediated phosphorylation of MLKL.

Akt activation is regulated, in part, by the level of PIP_3 which recruits it along with the PDPK1 (phosphoinositide-dependent protein kinase 1) to the cell membrane, where PDPK1 phosphorylates Akt to activate it.[110] The levels of PIP_3 are regulated by the balance between the opposing actions of PI3K's which phosphorylate PIP_2 to form PIP_3, and PTEN, which dephosphorylates PIP_3, converting it back to PIP_2.[111] PTEN has been shown to be a central factor for tumor suppression and a master regulator of homeostasis in eukaryotes,[112–119] regulating multiple cellular processes including proliferation, growth, metabolism, and survival.[120,121] PTEN inhibition has been shown to protect against myocardial infarction and cardiac, hepatic and cerebral ischemia/reperfusion (I/R) injuries.[122–124] These protective effects of PTEN inhibition involve increased levels of PIP_3, driving Akt activation and downregulation of cell death pathways. Our data demonstrates that PTEN inhibition, leading to Akt activation, can similarly lead to protection of macrophages against necroptosis and that

Figure 5 Continued. PDZK1$^{KO/KO}$LDLR$^{KO/KO}$ BM were fed the atherogenic HFD for 10 weeks. **A**, Representative images of H&E-stained aortic sinus atherosclerotic plaques. Quantification of (**B** and **D**) plaque volumes and (**C** and **E**) necrotic core areas for males (**B** and **C**) and females (**D** and **E**), respectively. **F** through **J**, Immunofluorescence staining for RIPK3 and MLKL phosphorylation in atherosclerotic plaques. **F** and **I**, Representative images of DAPI (blue), phospho-RIPK3 (green), phospho-MLKL (red), and merged images of atherosclerotic plaques from male (**F**) and female (**I**) PDZK1$^{KO/KO}$LDLR$^{KO/KO}$ mice transplanted with PDZK1$^{WT/WT}$LDLR$^{KO/KO}$ or PDZK1$^{KO/KO}$LDLR$^{KO/KO}$ BM. Yellow dashed lines mark atherosclerotic plaques. **G**, **H**, **J**, and **K**, Quantification of pRIPK3 and pMLKL immunofluorescence. n=6–7 individual mice (biological replicates) per group. Data were first subjected to the D'Agostino-Pearson test for normality and for equal variances. Data are means±SEM. Statistical analysis was done using unpaired Student *t*-test.

this may represent a strategy to attenuate necrotic core formation within atherosclerotic plaques. However, further studies are required to test this in vivo.

Although we explored the contribution of HDL to the protection of macrophages against necroptosis in vitro, and the ability of modulating ApoA1 levels to protection against necrotic core formation in vivo in the HFD fed ApoA1$^{KO/KO}$LDLR$^{KO/KO}$ and hApoA1$^{TG/TG}$LDLR$^{KO/KO}$ mice, it is important to point out that we cannot rule out the possible contributions of the altered levels of non-HDL cholesterol to the effects on atherosclerosis, and necroptosis and necrotic core development in atherosclerotic plaques. Further studies are required to evaluate the contribution of increased non-HDL cholesterol to the protection against necroptosis and necrotic core development observed in the HFD fed hApoA1$^{TG/TG}$LDLR$^{KO/KO}$ mice and the effects of the reduced levels of non-HDL cholesterol to the increased necroptosis and necrotic core development observed in the HFD-fed ApoA1$^{KO/KO}$LDLR$^{KO/KO}$ mice.

Nevertheless, this study advances our understanding of the pathways by which HDL can protect against atherosclerotic plaque development by demonstrating that HDL attenuates macrophage necroptosis by activating Akt signaling in macrophages in an SR-B1 and PDZK1-dependent manner and suggest that this may contribute to attenuating the development of necrotic cores within atherosclerotic plaques.

ARTICLE INFORMATION

Received June 16, 2021; accepted October 27, 2022.

Affiliations

Thrombosis and Atherosclerosis Research Institute, Department of Biochemistry and Biomedical Sciences, McMaster University, and Hamilton Health Sciences, Ontario, Canada.

Acknowledgments

The authors thank Dr Guinever Imperio for help with the graphical abstract. Designed the experiments (B.L. Trigatti, G.E.G. Kluck), carried out in vitro and in vivo experiments (G.E.G. Kluck, A.S. Qian, E.H. Sakarya, and H. Quach), managed mouse colony (Y.D. Deng), analyzed the data (G.E.G. Kluck), wrote and revised the article (B.L. Trigatti, G.E.G. Kluck, A.S. Qian, E.H. Sakarya).

Sources of Funding

This research was supported by a grant (PJT-162272) from the Canadian Institutes of Health Research (CIHR) to B.L. Trigatti.

Disclosures

None.

Supplemental Material

Expanded Materials and Methods
Figures S1–S11
Major Resources Table

REFERENCES

1. WHO CVD Risk Chart Working. World Health Organization cardiovascular disease risk charts: revised models to estimate risk in 21 global regions. *Lancet Glob Heal.* 2019;7:e1332–e1345. doi: 10.1016/S2214-109X(19)30318-3
2. Mozaffarian D, Benjamin EJ, Go AS, Arnett DK, Blaha MJ, Cushman M, Das SR, de Ferranti S, Després J-P, Fullerton HJ, et al; Writing Group Members; American Heart Association Statistics Committee; Stroke Statistics Subcommittee. Heart disease and stroke statistics-2016 update: a report from the American Heart Association. *Circulation.* 2016;133:e38–360. doi: 10.1161/CIR.0000000000000350
3. Otsuka F, Yasuda S, Noguchi T, Ishibashi-Ueda H. Pathology of coronary atherosclerosis and thrombosis. *Cardiovasc Diagn Ther.* 2016;6:396–408. doi: 10.21037/cdt.2016.06.01
4. Virmani R, Kolodgie FD, Burke AP, Farb A, Schwartz SM. Lessons from sudden coronary death: a comprehensive morphological classification scheme for atherosclerotic lesions. *Arterioscler Thromb Vasc Biol.* 2000;20:1262–1275. doi: 10.1161/01.atv.20.5.1262
5. Finn AV, Nakano M, Narula J, Kolodgie FD, Virmani R. Concept of vulnerable/unstable plaque. *Arterioscler Thromb Vasc Biol.* 2010;30:1282–1292. doi:10.1161/ATVBAHA.108.179739
6. Thorp E, Subramanian M, Tabas I. The role of macrophages and dendritic cells in the clearance of apoptotic cells in advanced atherosclerosis. *Eur J Immunol.* 2011;41:2515–2518. doi: 10.1002/eji.201141719
7. Ross R. Atherosclerosis - an inflammatory disease. *N Engl J Med.* 1999;340:115–126. doi: 10.1056/NEJM199901143400207
8. Falk E, Shah PK, Fuster V. Coronary plaque disruption. *Circulation.* 1995;92:657–671. doi: 10.1161/01.cir.92.3.657
9. Gonzalez L, Trigatti BL. Macrophage apoptosis and necrotic core development in atherosclerosis: a rapidly advancing field with clinical relevance to imaging and therapy. *Can J Cardiol.* 2017;33:303–312. doi:10.1016/j.cjca.2016.12.010
10. Roos A, Xu W, Castellano G, Nauta AJ, Garred P, Daha MR, van Kooten C. Mini-review: a pivotal role for innate immunity in the clearance of apoptotic cells. *Eur J Immunol.* 2004;34:921–929. doi: 10.1002/eji.200424904
11. Martinet W, Kockx MM. Apoptosis in atherosclerosis: focus on oxidized lipids and inflammation. *Curr Opin Lipidol.* 2001;12:535–41. doi:10.1097/00041433-200110000-00009
12. Kolodgie FD, Narula J, Burke AP, Haider N, Farb A, Hui-Liang Y, Smialek J, Virmani R. Localization of apoptotic macrophages at the site of plaque rupture in sudden coronary death. *Am J Pathol.* 2000;157:1259–1268. doi: 10.1016/S0002-9440(10)64641-X
13. Vandenabeele P, Galluzzi L, Vanden Berghe T, Kroemer G. Molecular mechanisms of necroptosis: an ordered cellular explosion. *Nat Rev Mol Cell Biol.* 2010;11:700–714. doi: 10.1038/nrm2970
14. Karunakaran D, Geoffrion M, Wei L, Gan W, Richards L, Shangari P, DeKemp EM, Beanlands RA, Perisic L, Maegdefessel L, et al. Targeting macrophage necroptosis for therapeutic and diagnostic interventions in atherosclerosis. *Sci Adv.* 2016;2:e1600224. doi: 10.1126/sciadv.1600224
15. Kaczmarek A, Vandenabeele P, Necroptosis KDV. The release of damage-associated molecular patterns and its physiological relevance. *Immunity.* 2013;38:209–223. doi: 10.1016/j.immuni.2013.02.003
16. Wang H, Sun L, Su L, Rizo J, Liu L, Wang L-F, Wang F-S, Wang X. Mixed lineage kinase domain-like protein MLKL causes necrotic membrane disruption upon phosphorylation by RIP3. *Mol Cell.* 2014;54:133–146. doi: 10.1016/j.molcel.2014.03.003
17. Dhuriya YK, Sharma D. Necroptosis: a regulated inflammatory mode of cell death. *J Neuroinflammation.* 2018;15: doi: 10.1186/s12974-018-1235-0
18. Linkermann A, Green DR. Necroptosis. *N Engl J Med.* 2014;370:455–465. doi: 10.1056/NEJMra1310050
19. Feoktistova M, Leverkus M. Programmed necrosis and necroptosis signalling. *FEBS J.* 2015;282:19–31. doi: 10.1111/febs.13120
20. Wu J, Huang Z, Ren J, Zhang Z, He P, Li Y, Ma J, Chen W, Zhang Y, Zhou X, et al. Mlkl knockout mice demonstrate the indispensable role of Mlkl in necroptosis. *Cell Res.* 2013;23:994–1006. doi: 10.1038/cr.2013.91
21. Lin J, Li H, Yang M, Ren J, Huang Z, Han F, Huang J, Ma J, Zhang D, Zhang Z, et al. A role of RIP3-mediated macrophage necrosis in atherosclerosis development. *Cell Rep.* 2013;3:200–210. doi: 10.1016/j.celrep.2012.12.012
22. Meng L, Jin W, Wang X. RIP3-mediated necrotic cell death accelerates systematic inflammation and mortality. *Proc Natl Acad Sci USA.* 2015;112:11007–11012. doi: 10.1073/pnas.1514730112
23. Thorp E, Tabas I. Mechanisms and consequences of efferocytosis in advanced atherosclerosis. *J Leukoc Biol.* 2009;86:1089–1095. doi: 10.1189/jlb.0209115
24. Gerlach BD, Marinello M, Heinz J, Rymut N, Sansbury BE, Riley CO, Sadhu S, Hosseini Z, Kojima Y, Tang DD, et al. Resolvin D1 promotes the targeting and clearance of necroptotic cells. *Cell Death Differ.* 2020;27:525–539. doi: 10.1038/s41418-019-0370-1
25. Gordon DJ, Knoke J, Probstfield JL, Superko R, Tyroler HA. High-density lipoprotein cholesterol and coronary heart disease in hypercholesterolemic men: the lipid research clinics coronary primary prevention trial. *Circulation.* 1986;74:1217–1225. doi: 10.1161/01.cir.74.6.1217

26. Gordon DJ, Probstfield JL, Garrison RJ, Neaton JD, Castelli WP, Knoke JD, Jacobs DR, Bangdiwala S, Tyroler HA. High-density lipoprotein cholesterol and cardiovascular disease. Four prospective American studies. *Circulation.* 1989;79:8–15. doi: 10.1161/01.cir.79.1.8
27. Pekkanen J, Linn S, Heiss G, Suchindran CM, Leon A, Rifkind BM, Tyroler HA. Ten-year mortality from cardiovascular disease in relation to cholesterol level among men with and without preexisting cardiovascular disease. *N Engl J Med.* 1990;322:1700–1707. doi: 10.1056/NEJM199006143222403
28. Pedersen TR, Olsson AG, Færgeman O, Kjekshus J, Wedel H, Berg K, Wilhelmsen L, Haghfelt T, Thorgeirsson G, Pyörälä K, et al. Lipoprotein changes and reduction in the incidence of major coronary heart disease events in the Scandinavian Simvastatin Survival Study (4S). *Circulation.* 1998;97:1453–1460. doi: 10.1161/01.cir.97.15.1453
29. Sacks FM, Tonkin AM, Shepherd J, Braunwald E, Cobbe S, Hawkins CM, Keech A, Packard C, Simes J, Byington R, et al. Effect of pravastatin on coronary disease events in subgroups defined by coronary risk factors: the prospective pravastatin pooling project. *Circulation.* 2000;102:1893–1900. doi: 10.1161/01.cir.102.16.1893
30. Simes RJ, Marschner IC, Hunt D, Colquhoun D, Sullivan D, Stewart RAH, Hague W, Keech A, Thompson P, White H, et al; LIPID Study Investigators. Relationship between lipid levels and clinical outcomes in the long-term Intervention with Pravastatin in Ischemic Disease (LIPID) trial: to what extent is the reduction in coronary events with pravastatin explained by on-study lipid levels?. *Circulation.* 2002;105:1162–1169. doi: 10.1161/hc1002.105136
31. Barter P, Gotto AM, LaRosa JC, Maroni J, Szarek M, Grundy SM, Kastelein JJP, Bittner V, Fruchart J-C; Treating to New Targets Investigators. HDL cholesterol, very low levels of LDL cholesterol, and cardiovascular events. *N Engl J Med.* 2007;357:1301–1310. doi: 10.1056/NEJMoa064278
32. LaRosa JC, Grundy SM, Waters DD, Shear C, Barter P, Fruchart J-C, Gotto AM, Greten H, Kastelein JJP, Shepherd J, et al; Treating to New Targets (TNT) Investigators. Intensive lipid lowering with atorvastatin in patients with stable coronary disease. *N Engl J Med.* 2005;352:1425–1435. doi: 10.1056/NEJMoa050461
33. LaRosa JC, Grundy SM, Kastelein JJP, Kostis JB, Greten H; Treating to New Targets (TNT) Steering Committee and InvestigatorsTreating to New Targets (TNT) Steering Committee and Investigators. Safety and efficacy of Atorvastatin-induced very low-density lipoprotein cholesterol levels in patients with coronary heart disease (a post hoc analysis of the treating to new targets [TNT] study). *Am J Cardiol.* 2007;100:747–752. doi: 10.1016/j.amjcard.2007.03.102
34. Arsenault BJ, Barter P, DeMicco DA, Bao W, Preston GM, LaRosa JC, Grundy SM, Deedwania P, Greten H, Wenger NK, et al; TNT Study Investigators. Prediction of cardiovascular events in statin-treated stable coronary patients by lipid and nonlipid biomarkers. *J Am Coll Cardiol.* 2011; 57:63–69. doi: 10.1016/j.jacc.2010.06.052
35. Badimon JJ, Badimon L, Fuster V. Regression of atherosclerotic lesions by high density lipoprotein plasma fraction in the cholesterol-fed rabbit. *J Clin Invest.* 1990;85:1234–1241. doi: 10.1172/JCI114558
36. Beitz J, Beitz A, Antonov IV, Misharin AY, Mest HJ. Does a HDL injection reduce the development of serum hyperlipidemia and progression of fatty streaks in cholesterol fed rabbits?. *Prostaglandins Leukot Essent Fatty Acids.* 1992;47:149–152. doi: 10.1016/0952-3278(92)90152-9
37. Rubin EM, Krauss RM, Spangler EA, Verstuyft JG, Clift SM. Inhibition of early atherogenesis in transgenic mice by human apolipoprotein AI. *Nature.* 1991;353:265–267. doi: 10.1038/353265a0
38. Schultz JR, Verstuyft JG, Gong EL, Nichols AV, Rubin EM. Protein composition determines the anti-atherogenic properties of HDL in transgenic mice. *Nature.* 1993;365:762–764. doi: 10.1038/365762a0
39. Plump AS, Scott CJ, Breslow JL. Human apolipoprotein A-I gene expression increases high density lipoprotein and suppresses atherosclerosis in the apolipoprotein E-deficient mouse. *Proc Natl Acad Sci USA.* 1994;91:9607–9611. doi: 10.1073/pnas.91.20.9607
40. Patel S, Di Bartolo BA, Nakhla S, Heather AK, Mitchell TW, Jessup W, Celermajer DS, Barter PJ, Rye K-A. Anti-inflammatory effects of apolipoprotein A-I in the rabbit. *Atherosclerosis.* 2010;212:392–397. doi: 10.1016/j.atherosclerosis.2010.05.035
41. Di Bartolo BA, Vanags LZ, Tan JT, Bao S, Rye K-A, Barter PJ, Bursill CA. The apolipoprotein A-I mimetic peptide, ETC-642, reduces chronic vascular inflammation in the rabbit. *Lipids Health Dis.* 2011;10:224. doi: 10.1186/1476-511X-10-224
42. Vuilleumier N, Dayer J-M, von Eckardstein A, Roux-Lombard P. Pro- or anti-inflammatory role of apolipoprotein A-1 in high-density lipoproteins?. *Swiss Med Wkly.* 2013;143:w13781. doi: 10.4414/smw.2013.13781
43. Tchoua U, D'Souza W, Mukhamedova N, Blum D, Niesor E, Mizrahi J, Maugeais C, Sviridov D. The effect of cholesteryl ester transfer protein overexpression and inhibition on reverse cholesterol transport. *Cardiovasc Res.* 2008;77:732–739. doi: 10.1093/cvr/cvm087
44. Moore RE, Navab M, Millar JS, Zimetti F, Hama S, Rothblat GH, Rader DJ. Increased atherosclerosis in mice lacking apolipoprotein A-I attributable to both impaired reverse cholesterol transport and increased inflammation. *Circ Res.* 2005;97:763–771. doi: 10.1161/01.RES.0000185320.82962.F7
45. Zhang YZ, Zanotti I, Reilly MP, Glick JM, Rothblat GH, Rader DJ. Overexpression of apolipoprotein A-I promotes reverse transport of cholesterol from macrophages to feces in vivo. *Circulation.* 2003;108:661–663. doi: 10.1161/01.cir.0000086981.09834.e0
46. Tanigawa H, Billheimer JT, Tohyama JI, Zhang YZ, Rothblat G, Rader DJ. Expression of cholesteryl ester transfer protein in mice promotes macrophage reverse cholesterol transport. *Circulation.* 2007;116:1267–1273. doi: 10.1161/CIRCULATIONAHA.107.704254
47. Trajkovska KT, Topuzovska S. High-density lipoprotein metabolism and reverse cholesterol transport: strategies for raising HDL cholesterol. *Anatol J Cardiol.* 2017;18:149–154. doi: 10.14744/AnatolJCardiol.2017.7608
48. Ouimet M, Barrett TJ, Fisher EA. HDL and reverse cholesterol transport: basic mechanisms and their roles in vascular health and disease. *Circ Res.* 2019;124:1505–1518. doi: 10.1161/CIRCRESAHA.119.312617
49. Schill RL, Knaack DA, Powers HR, Chen Y, Yang M, Schill DJ, Silverstein RL, Sahoo D. Modification of HDL by reactive aldehydes alters select cardioprotective functions of HDL in macrophages. *FEBS J.* 2020;287:695–707. doi: 10.1111/febs.15034
50. Chadwick AC, Holme RL, Chen Y, et al. Acrolein impairs the cholesterol transport functions of high density lipoproteins. *PLoS One.* 2015;10:e0123138. doi: 10.1371/journal.pone.0123138
51. Nofer JR. Signal transduction by HDL: agonists, receptors, and signaling cascades. In: *Handbook of Experimental Pharmacology.* Springer New York LLC. 2015; 224:229–256. doi:10.1007/978-3-319-09665-0_6
52. Trigatti BL, Fuller M. HDL signaling and protection against coronary artery atherosclerosis in mice. *J Biomed Res.* 2016;30:94–100. doi:10.7555/JBR.30.20150079
53. Seetharam D, Mineo C, Gormley AK, Gibson LL, Vongpatanasin W, Chambliss KL, Hahner LD, Cummings ML, Kitchens RL, Marcel YL, et al. High-density lipoprotein promotes endothelial cell migration and reendothelialization via scavenger receptor-B type I. *Circ Res.* 2006;98:63–72. doi: 10.1161/01.RES.0000199272.59432.5b
54. Al-Jarallah A, Trigatti BL. A role for the scavenger receptor, class B type I in high density lipoprotein dependent activation of cellular signaling pathways. *Biochim Biophys Acta Mol Cell Biol Lipids.* 2010;1801:1239–1248. doi: 10.1016/j.bbalip.2010.08.006
55. Mineo C, Shaul PW. Novel biological functions of high-density lipoprotein cholesterol. *Circ Res.* 2012;111:1079–1090. doi: 10.1161/CIRCRESAHA.111.258673
56. Yu P, Qian AS, Chathely KM, Trigatti BL. PDZK1 in leukocytes protects against cellular apoptosis and necrotic core development in atherosclerotic plaques in high fat diet fed ldl receptor deficient mice. *Atherosclerosis.* 2018;276:171–181. doi: 10.1016/j.atherosclerosis.2018.05.009
57. Yu P, Qian AS, Chathely KM, Trigatti BL. Data on leukocyte PDZK1 deficiency affecting macrophage apoptosis but not monocyte recruitment, cell proliferation, macrophage abundance or ER stress in atherosclerotic *plaques of LDLR deficient mice. Data Br.* 2018;19:1148–1161. doi: 10.1016/j.dib.2018.05.128
58. Kocher O, Birrane G, Tsukamoto K, Fenske S, Yesilaltay A, Pal R, Daniels K, Ladias JAA, Krieger M. In vitro and in vivo analysis of the binding of the C terminus of the HDL receptor scavenger receptor class B, type I (SR-BI), to the PDZ1 domain of its adaptor protein PDZK1. *J Biol Chem.* 2010;285:34999–35010. doi: 10.1074/jbc.M110.164418
59. Kocher O, Yesilaltay A, Shen CH, Zhang S, Daniels K, Pal R, Chen J, Krieger M. Influence of PDZK1 on lipoprotein metabolism and atherosclerosis. *Biochim Biophys Acta Mol Basis Dis.* 2008;1782:310–316. doi: 10.1016/j.bbadis.2008.02.004
60. Kocher O, Pal R, Roberts M, Cirovic C, Gilchrist A. Targeted disruption of the PDZK1 gene by homologous recombination. *Mol Cell Biol.* 2003;23:1175–1180. doi: 10.1128/MCB.23.4.1175-1180.2003
61. Zhu W, Saddar S, Seetharam D, Chambliss KL, Longoria C, Silver DL, Yuhanna IS, Shaul PW, Mineo C. The scavenger receptor class B type I adaptor protein PDZK1 maintains endothelial monolayer integrity. *Circ Res.* 2008;102:480–487. doi: 10.1161/CIRCRESAHA.107.159079
62. Al-Jarallah A, Chen X, González L, Trigatti BL. High density lipoprotein stimulated migration of macrophages depends on the scavenger receptor class B, Type I, PDZK1 and Akt1 and is blocked by sphingosine

1 phosphate receptor antagonists. *PLoS One.* 2014;9:e106487. doi: 10.1371/journal.pone.0106487
63. Covey SD, Krieger M, Wang W, Penman M, Trigatti BL. Scavenger receptor class B type I-mediated protection against atherosclerosis in LDL receptor-negative mice involves its expression in bone marrow-derived cells. *Arterioscler Thromb Vasc Biol.* 2003;23:1589–1594. doi: 10.1161/01.ATV.0000083343.19940.A0
64. Venegas-Pino DE, Banko N, Khan MI, Shi Y, Werstuck GH. Quantitative analysis and characterization of atherosclerotic lesions in the murine aortic sinus. *J Vis Exp.* 2013;82:50933. doi: 10.3791/50933
65. Wählby C, Erlandsson F, Bengtsson E, Zetterberg A. Sequential immunofluorescence staining and image analysis for detection of large numbers of antigens in individual cell nuclei. *Cytometry.* 2002;47:32–41. doi: 10.1002/cyto.10026
66. Zhang B, Uehara Y, Hida S, Miura S-ichiro, Rainwater DL, Segawa M, Kumagai K, Rye K-A, Saku K. Effects of reconstituted HDL on charge-based LDL subfractions as characterized by capillary isotachophoresis. *J Lipid Res.* 2007;48:1175–1189. doi: 10.1194/jlr.M600227-JLR200
67. Laemmli UK. Cleavage of structural proteins during the assembly of the head of bacteriophage T4. *Nature.* 1970;227:680–685. doi: 10.1038/227680a0
68. Towbin H, Staehelin T, Gordon J. Electrophoretic transfer of proteins from polyacrylamide gels to nitrocellulose sheets: procedure and some applications. *Proc Natl Acad Sci USA.* 1979;76:4350–4354. doi: 10.1073/pnas.76.9.4350
69. Boisvert WA, Black AS, Curtiss LK. ApoA1 reduces free cholesterol accumulation in atherosclerotic lesions of apoE-deficient mice transplanted with apoE-expressing macrophages. *Arterioscler Thromb Vasc Biol.* 1999;19:525–530. doi: 10.1161/01.atv.19.3.525
70. Hughes SD, Verstuyft J, Rubin EM. HDL deficiency in genetically engineered mice requires elevated LDL to accelerate atherogenesis. *Arterioscler Thromb Vasc Biol.* 1997;17:1725–1729. doi: 10.1161/01.atv.17.9.1725
71. Moore RE, Kawashiri M, Kitajima K, Secreto A, Millar JS, Pratico D, Rader DJ. Apolipoprotein A-I deficiency results in markedly increased atherosclerosis in mice lacking the LDL receptor. *Arterioscler Thromb Vasc Biol.* 2003;23:1914–1920. doi: 10.1161/01.ATV.0000092328.66882.F5
72. Zabalawi M, Bhat S, Loughlin T, Thomas MJ, Alexander E, Cline M, Bullock B, Willingham M, Sorci-Thomas MG. Induction of fatal inflammation in LDL receptor and apoA-I double-knockout mice fed dietary fat and cholesterol. *Am J Pathol.* 2003;163:1201–1213. doi: 10.1016/S0002-9440(10)63480-3
73. Takahashi N, Duprez L, Grootjans S, Cauwels A, Nerinckx W, DuHadaway JB, Goossens V, Roelandt R, Van Hauwermeiren F, Libert C, et al. Necrostatin-1 analogues: Critical issues on the specificity, activity and in vivo use in experimental disease models. *Cell Death Dis.* 2012;3:e437–e437. doi: 10.1038/cddis.2012.176
74. Yesilaltay A, Daniels K, Pal R, Krieger M, Kocher O. Loss of PDZK1 causes coronary artery occlusion and myocardial infarction in paigen diet-fed apolipoprotein E deficient mice. Leri A, ed. *PLoS One.* 2009;4:e8103. doi: 10.1371/journal.pone.0008103
75. Zabalawi M, Bhat S, Loughlin T, Thomas MJ, Alexander E, Cline M, Bullock B, Willingham M, Sorci-Thomas MG. Induction of fatal inflammation in LDL receptor and ApoA-I double-knockout mice fed dietary fat and cholesterol. *Am J Pathol.* 2003;163:1201–1213. doi: 10.1016/S0002-9440(10)63480-3
76. Busnelli M, Manzini S, Colombo A, Franchi E, Bonacina F, Chiara M, Arnaboldi F, Donetti E, Ambrogi F, Oleari R, et al. Lack of ApoA-I in ApoEKO mice causes skin xanthomas, worsening of inflammation, and increased coronary atherosclerosis in the absence of hyperlipidemia. *Arterioscler Thromb Vasc Biol.* 2022;42:839–856. doi: 10.1161/ATVBAHA.122.317790
77. Rubin EM, Krauss RM, Spangler EA, Verstuyft JG, Clift SM. Inhibition of early atherogenesis in transgenic mice by human apolipoprotein AI. *Nature.* 1991;353:265–267. doi: 10.1038/353265a0
78. Méndez-Lara KA, Farré N, Santos D, et al. Human ApoA-I overexpression enhances macrophage-specific reverse cholesterol transport but fails to prevent inherited diabesity in mice. *Int J Mol Sci.* 2019;20: doi: 10.3390/IJMS20030655
79. Zhu W, Saddar S, Seetharam D, Chambliss KL, Longoria C, Silver DL, Yuhanna IS, Shaul PW, Mineo C. The scavenger receptor class B type I adaptor protein PDZK1 maintains endothelial monolayer integrity. *Circ Res.* 2008;102:480–487. doi: 10.1161/CIRCRESAHA.107.159079
80. Assanasen C, Mineo C, Seetharam D, Yuhanna IS, Marcel YL, Connelly MA, Williams DL, de la Llera-Moya M, Shaul PW, Silver DL. Cholesterol binding, efflux, and a PDZ-interacting domain of scavenger receptor–BI mediate HDL-initiated signaling. *J Clin Invest.* 2005;115:969–977. doi: 10.1172/JCI23858
81. Al-Jarallah A, Chen X, González L, Trigatti BL. High density lipoprotein stimulated migration of macrophages depends on the scavenger receptor class B, Type I, PDZK1 and Akt1 and is blocked by sphingosine 1 phosphate receptor antagonists. kocher O, ed. *PLoS One.* 2014;9:e106487. doi: 10.1371/journal.pone.0106487
82. Gao M, Zhao D, Schouteden S, Sorci-Thomas MG, Van Veldhoven PP, Eggermont K, Liu G, Verfaillie CM, Feng Y. Regulation of high-density lipoprotein on hematopoietic stem/progenitor cells in atherosclerosis requires scavenger receptor type BI expression. *Arterioscler Thromb Vasc Biol.* 2014;34:1900–1909. doi: 10.1161/ATVBAHA.114.304006
83. Zhang Y, Ahmed AM, McFarlane N, Capone C, Boreham DR, Truant R, Igdoura SA, Trigatti BL. Regulation of SR-BI-mediated selective lipid uptake in Chinese hamster ovary-derived cells by protein kinase signaling pathways. *J Lipid Res.* 2007;48:405–416. doi: 10.1194/jlr.M600326-JLR200
84. Mineo C, Yuhanna IS, Quon MJ, Shaul PW. High density lipoprotein-induced endothelial nitric-oxide synthase activation is mediated by Akt and MAP kinases. *J Biol Chem.* 2003;278:9142–9149. doi: 10.1074/jbc.M211394200
85. Durham KK, Chathely KM, Trigatti BL. High-density lipoprotein protects cardiomyocytes against necrosis induced by oxygen and glucose deprivation through SR-B1, PI3K, and AKT1 and 2. *Biochem J.* 2018;475:1253–1265. doi: 10.1042/BCJ20170703
86. Yuhanna IS, Zhu Y, Cox BE, Hahner LD, Osborne-Lawrence S, Lu P, Marcel YL, Anderson RG, Mendelsohn ME, Hobbs HH, et al. High-density lipoprotein binding to scavenger receptor-BI activates endothelial nitric oxide synthase. *Nat Med.* 2001;7:853–857. doi: 10.1038/89986
87. Assanasen C, Mineo C, Seetharam D, Yuhanna IS, Marcel YL, Connelly MA, Williams DL, de la Llera-Moya M, Shaul PW, Silver DL. Cholesterol binding, efflux, and a PDZ-interacting domain of scavenger receptor-BI mediate HDL-initiated signaling. *J Clin Invest.* 2005;115:969–977. doi: 10.1172/JCI23858
88. Silke J, Rickard JA, Gerlic M. The diverse role of RIP kinases in necroptosis and inflammation. *Nat Immunol.* 2015;16:689–697. doi: 10.1038/ni.3206
89. Wegner KW, Saleh D, Degterev A. Complex pathologic roles of RIPK1 and RIPK3: moving beyond necroptosis. *Trends Pharmacol Sci.* 2017;38:202–225. doi: 10.1016/j.tips.2016.12.005
90. Ofengeim D, Yuan J. Regulation of RIP1 kinase signalling at the crossroads of inflammation and cell death. *Nat Rev Mol Cell Biol.* 2013;14:727–736. doi: 10.1038/nrm3683
91. Festjens N, Vanden Berghe T, Cornelis S, Vandenabeele P. RIP1, a kinase on the crossroads of a cell's decision to live or die. *Cell Death Differ.* 2007;14:400–410. doi: 10.1038/sj.cdd.4402085
92. Degterev A, Ofengeim D, Yuan J. Targeting RIPK1 for the treatment of human diseases. *Proc Natl Acad Sci USA.* 2019;116:9714–9722. doi: 10.1073/pnas.1901179116
93. Delanghe T, Dondelinger Y, Bertrand MJM. RIPK1 kinase-dependent death: a symphony of phosphorylation events. *Trends Cell Biol.* 2020;30:189–200. doi: 10.1016/j.tcb.2019.12.009
94. Li J, McQuade T, Siemer AB, Napetschnig J, Moriwaki K, Hsiao Y-S, Damko E, Moquin D, Walz T, McDermott A, et al. The RIP1/RIP3 necrosome forms a functional amyloid signaling complex required for programmed necrosis. *Cell.* 2012;150:339–350. doi: 10.1016/j.cell.2012.06.019
95. Sun L, Wang H, Wang Z, He S, Chen S, Liao D, Wang L, Yan J, Liu W, Lei X, et al. Mixed lineage kinase domain-like protein mediates necrosis signaling downstream of RIP3 kinase. *Cell.* 2012;148:213–227. doi: 10.1016/j.cell.2011.11.031
96. Lafont E, Draber P, Rieser E, Reichert M, Kupka S, de Miguel D, Draberova H, von Mässenhausen A, Bhamra A, Henderson S, et al. TBK1 and IKKε prevent TNF-induced cell death by RIPK1 phosphorylation. *Nat Cell Biol.* 2018;20:1389–1399. doi: 10.1038/s41556-018-0229-6
97. Heger K, Dixit VM. TBK1 and IKKε restrain cell death. *Nat Cell Biol.* 2018;20:1330–1331. doi: 10.1038/s41556-018-0239-4
98. Dondelinger Y, Jouan-Lanhouet S, Divert T, Theatre E, Bertin J, Gough PJ, Giansanti P, Heck AJR, Dejardin E, Vandenabeele P, et al. NF-κB-Independent Role of IKKα/IKKβ in preventing RIPK1 kinase-dependent apoptotic and necroptotic cell death during TNF signaling. *Mol Cell.* 2015;60:63–76. doi: 10.1016/j.molcel.2015.07.032
99. Koppe C, Verheugd P, Gautheron J, Reisinger F, Kreggenwinkel K, Roderburg C, Quagliata L, Terracciano L, Gassler N, Tolba RH, et al. IκB kinaseα/β control biliary homeostasis and hepatocarcinogenesis in mice by phosphorylating the cell-death mediator receptor-interacting protein kinase 1. *Hepatology.* 2016;64:1217–1231. doi: 10.1002/hep.28723
100. Jaco I, Annibaldi A, Lalaoui N, Wilson R, Tenev T, Laurien L, Kim C, Jamal K, Wicky John S, Liccardi G, et al. MK2 phosphorylates RIPK1

to prevent TNF-induced cell death. *Mol Cell.* 2017;66:698–710.e5. doi: 10.1016/j.molcel.2017.05.003
101. Yuan J, Amin P, Ofengeim D. Necroptosis and RIPK1-mediated neuroinflammation in CNS diseases. *Nat Rev Neurosci.* 2019;20:19–33. doi: 10.1038/s41583-018-0093-1
102. Ozes ON, Mayo LD, Gustin JA, Pfeffer SR, Pfeffer LM, Donner DB. NF-κB activation by tumour necrosis factor requires tie Akt serine- threonine kinase. *Nature.* 1999;401:82–85. doi: 10.1038/43466
103. Madrid LV, Wang C-Y, Guttridge DC, Schottelius AJG, Baldwin AS, Mayo MW. Akt suppresses apoptosis by stimulating the transactivation potential of the RelA/p65 subunit of NF-κB. *Mol Cell Biol.* 2000;20:1626–1638. doi: 10.1128/MCB.20.5.1626-1638.2000
104. Factor V, Oliver AL, Panta GR, Thorgeirsson SS, Sonenshein GE, Arsura M. Roles of Akt/PKB and IKK complex in constitutive induction of NF-κB in hepatocellular carcinomas of transforming growth factor α/c-myc transgenic mice. *Hepatology.* 2001;34:32–41. doi: 10.1053/jhep.2001.25270
105. Bai D, Ueno L, Vogt PK. Akt-mediated regulation of NFκB and the essentialness of NFκB for the oncogenicity of PI3K and Akt. *Int J Cancer.* 2009;125:2863–2870. doi: 10.1002/ijc.24748
106. Sun ZJ, Chen G, Hu X, Zhang W, Liu Y, Zhu L-X, Zhou Q, Zhao Y-F. Activation of PI3K/Akt/IKK-α/NF-κB signaling pathway is required for the apoptosis-evasion in human salivary adenoid cystic carcinoma: Its inhibition by quercetin. *Apoptosis.* 2010;15:850–863. doi: 10.1007/s10495-010-0497-5
107. Ouyang C, Nie L, Gu M, Wu A, Han X, Wang X, Shao J, Xia Z. Transforming growth factor (TGF)-β-activated kinase 1 (TAK1) activation requires phosphorylation of serine 412 by protein kinase A catalytic subunit α (PKACα) and X-linked protein kinase (PRKX). *J Biol Chem.* 2014;289:24226–24237. doi: 10.1074/jbc.M114.559963
108. Dovey CM, Diep J, Clarke BP, Hale AT, McNamara DE, Guo H, Brown NW, Cao JY, Grace CR, Gough PJ, et al. MLKL requires the inositol phosphate code to execute necroptosis. *Mol Cell.* 2018;70:936–948.e7. doi: 10.1016/j.molcel.2018.05.010
109. McNamara DE, Dovey CM, Hale AT, Quarato G, Grace CR, Guibao CD, Diep J, Nourse A, Cai CR, Wu H, et al. Direct activation of human MLKL by a select repertoire of inositol phosphate metabolites. *Cell Chem Biol.* 2019;26:863–877.e7. doi: 10.1016/j.chembiol.2019.03.010
110. Stephens L, Anderson K, Stokoe D, Erdjument-Bromage H, Painter GF, Holmes AB, Gaffney PR, Reese CB, McCormick F, Tempst P, et al. Prohtein kinase B kinases that mediate phosphatidylinositol 3,4,5- trisphosphate-dependent activation of protein kinase B. *Science.* 1998;279:710–714. doi: 10.1126/science.279.5351.710
111. Auger KR, Serunian LA, Soltoff SP, Libby P, Cantley LC. PDGF-dependent tyrosine phosphorylation stimulates production of novel polyphosphoinositides in intact cells. *Cell.* 1989;57:167–175. doi: 10.1016/0092-8674(89)90182-7
112. Cid VJ, Rodríguez-Escudero I, Andrés-Pons A, Romá-Mateo C, Gil A, den Hertog J, Molina M, Pulido R. Assessment of PTEN tumor suppressor activity in nonmammalian models: the year of the yeast. *Oncogene.* 2008;27:5431–5442. doi: 10.1038/onc.2008.240
113. Correia NC, Gírio A, Antunes I, Martins LR, Barata JT. The multiple layers of non-genetic regulation of PTEN tumour suppressor activity. *Eur J Cancer.* 2014;50:216–225. doi: 10.1016/j.ejca.2013.08.017
114. Hopkins BD, Hodakoski C, Barrows D, Mense SM, Parsons RE. PTEN function: the long and the short of it. *Trends Biochem Sci.* 2014;39:183–190. doi: 10.1016/j.tibs.2014.02.006
115. Leslie NR, Foti M. Non-genomic loss of PTEN function in cancer: not in my genes. *Trends Pharmacol Sci.* 2011;32:131–40. doi:10.1016/j.tips.2010.12.005
116. Shi Y, Paluch BE, Wang X, Jiang X. PTEN at a glance. *J Cell Sci.* 2012;125:4687–4692. doi: 10.1242/jcs.093765
117. Song MS, Salmena L, Pandolfi PP. The functions and regulation of the PTEN tumour suppressor. *Nat Rev Mol Cell Biol.* 2012;13:283–296. doi: 10.1038/nrm3330
118. Stambolic V, Suzuki A, De la Pompa JL, Brothers GM, Mirtsos C, Sasaki T, Ruland J, Penninger JM, Siderovski DP, Mak TW. Negative regulation of PKB/Akt-dependent cell survival by the tumor suppressor PTEN. *Cell.* 1998;95:29–39. doi: 10.1016/s0092-8674(00)81780-8
119. Sun H, Lesche R, Li DM, Liliental J, Zhang H, Gao J, Gavrilova N, Mueller B, Liu X, Wu H. PTEN modulates cell cycle progression and cell survival by regulating phosphatidylinositol 3,4,5,-trisphosphate and Akt/protein kinase B signaling pathway. *Proc Natl Acad Sci USA.* 1999;96:6199–6204. doi: 10.1073/pnas.96.11.6199
120. Worby CA, Dixon JE. Pten. *Annu Rev Biochem.* 2014;83:641–669. doi: 10.1146/annurev-biochem-082411-113907
121. Goberdhan DCI, Wilson C. PTEN: Tumour suppressor, multifunctional growth regulator and more. *Hum Mol Genet.* 2003;12:R239–R248. doi: 10.1093/hmg/ddg288
122. Dal Ponte C, Alchera E, Follenzi A, et al. Pharmacological postconditioning protects against hepatic ischemia/reperfusion injury. *Liver Transplant.* 2011;17:474–482. doi: 10.1002/lt.22256
123. Guo JY, Ding J, Yuan F, Chen H, Chen SW, Tian HL. Dose-dependent protective effect of bisperoxovanadium against acute cerebral ischemia in a rat model of ischemia/reperfusion injury. *Int J Mol Sci.* 2013;14:12013–12022. doi: 10.3390/ijms140612013
124. Keyes KT, Xu J, Long B, Zhang C, Hu Z, Ye Y. Pharmacological inhibition of PTEN limits myocardial infarct size and improves left ventricular function postinfarction. *Am J Physiol Hear Circ Physiol.* 2010;298:H1198–H1208. doi: 10.1152/ajpheart.00915.2009